A ubiquitin-proteasome pathway degrades the inner nuclear membrane protein Bqt4 to maintain nuclear membrane homeostasis

Toan Khanh Le[1], Yasuhiro Hirano[1,3], Haruhiko Asakawa[1,3], Koji Okamoto[2], Tatsuo Fukagawa[3], Tokuko Haraguchi[1] and Yasushi Hiraoka[1,*]

[1] Nuclear Dynamics Group, Graduate School of Frontier Biosciences, Osaka University, Suita 565-0871, Japan;

[2] Laboratory of Mitochondrial Dynamics, Graduate School of Frontier Biosciences, Osaka University, Suita 565-0871, Japan

[3] Laboratory of Chromosome Biology, Graduate School of Frontier Biosciences, Osaka University, Suita 565-0871, Japan

Running title: Bqt4 degradation pathway in NE

[*] **Corresponding to:**

Yasushi Hiraoka (hiraoka@fbs.osaka-u.ac.jp), Graduate School of Frontier Biosciences, Osaka University, 1-3 Yamadaoka, Suita 565-0871, Japan. Tel.: +81-6-6879-4621, FAX: +81-6-6789-4622

Keywords: Inner nuclear membrane, Protein degradation, Fission Yeast, Bqt3, Bqt4

Summary statement

Appropriate levels of the inner nuclear membrane protein Bqt4 are maintained by ubiquitin-proteasome-mediated degradation. Aberrant accumulation of Bqt4 disturbs nuclear membrane homeostasis.

Abstract

Aberrant accumulation of inner nuclear membrane (INM) proteins is associated with deformed nuclear morphology and mammalian diseases. However, the mechanisms underlying the maintenance of INM homeostasis remain poorly understood. In this study, we explored the degradation mechanisms of the INM protein, Bqt4, in the fission yeast *Schizosaccharomyces pombe*. We have previously shown that Bqt4 interacts with the transmembrane protein Bqt3 at the INM and is degraded in the absence of Bqt3. Here, we revealed that excess Bqt4, unassociated with Bqt3, was targeted for degradation by the ubiquitin-proteasome system localized in the nucleus and Bqt3 antagonized this process. The degradation process involved the Doa10 E3 ligase complex at the INM. Bqt4 is a tail-anchored protein and extraction from the membrane by the Cdc48 complex is required for its degradation. The C-terminal transmembrane domain of Bqt4 is necessary and sufficient for proteasome-dependent protein degradation. Accumulation of Bqt4 at the INM impaired cell viability with nuclear envelope deformation, suggesting that quantity control of Bqt4 plays an important role in nuclear membrane homeostasis.

Introduction

The eukaryotic nucleus is enclosed by the nuclear envelope (NE), which separates the nucleoplasm from the cytoplasm. The NE comprises inner and outer nuclear membranes (INM and ONM, respectively). The ONM is continuous with the endoplasmic reticulum (ER). The INM is involved in the organization and regulation of chromosomes by modulating chromatin potential for gene expression, DNA replication, DNA damage repair, and genome stability (Mekhail and Moazed, 2010; Hirano et al., 2020a; Pawar and Kutay, 2021). Excess amounts of INM proteins result in their aberrant accumulation at the NE, often causing nuclear deformation and malfunctioning (Gonzalez et al., 2012). The aberrant accumulation of INM proteins has been linked to certain mammalian diseases. For example, accumulation of the INM protein SUN1 was found to be pathogenic in human laminopathies such as Emery-Dreifuss muscular dystrophy and Hutchinson-Gilford progeria syndrome (Chen et al., 2012). Therefore, the amount of INM proteins must be regulated. However, the mechanisms that regulate levels of resident INM proteins to maintain INM homeostasis remain poorly understood.

Mechanisms for ER membrane homeostasis have been well studied: ER membrane proteins are regulated through the ER-associated degradation (ERAD) system, which is involved in degrading misfolded or mislocalized ER proteins as a means of protein quality control (Vembar and Brodsky, 2008; Ruggiano et al., 2014; Christianson and Carvalho, 2022). ERAD involves the ubiquitin-proteasome system (UPS), in which polyubiquitin chains are covalently attached to a substrate protein, leading to its recognition and degradation by the 26S proteasome complex. Ubiquitination reactions involve three different classes of enzymes: E1 ubiquitin-activating enzymes, E2 ubiquitin-conjugating enzymes, and E3 ubiquitin ligases, such as Hrd1 and Doa10 (human MARCHF6/TEB4). INM-associated degradation (INMAD) has been proposed as an extension of the ERAD to maintain INM

69 homeostasis, which also depends on the UPS (Foresti et al., 2014; Khmelinskii et al., 2014;
70 Koch and Yu, 2019; Smoyer and Jaspersen, 2019; Mannino and Lusk, 2022). It has been
71 shown that in the budding yeast *Saccharomyces cerevisiae*, ERAD and INMAD require
72 additional machinery for the degradation of integral membrane proteins, involving
73 Cdc48/p97, an ATPase associated with diverse cellular activities (AAA-ATPase), which
74 removes the ubiquitinated proteins from the membrane before transferring them to the
75 proteasome for degradation (Ruggiano et al., 2014; Christianson and Carvalho, 2022; Koch
76 and Yu, 2019; Smoyer and Jaspersen, 2019; Mannino and Lusk, 2022).
77 In the fission yeast *Schizosaccharomyces pombe*, several INM proteins have been
78 studied for their roles in the organization and regulation of chromosome stability, including
79 Ima1, Lem2, Man1, Bqt3, and Bqt4 (Chikashige et al., 2006; Chikashige et al., 2009; Hiraoka
80 et al., 2011; Steglich et al., 2012; Gonzalez et al., 2012; Tange et al., 2016; Hirano et al.,
81 2020b). In particular, we found that Bqt4 was degraded in the absence of Bqt3 (Chikashige et
82 al., 2009). Bqt3 is a transmembrane protein composed of seven transmembrane domains
83 (TMDs) along its entire length. Bqt4, which interacts with Bqt3, is predicted to be a tail-
84 anchored protein. Immunoelectron microscopy analysis has shown that Bqt3 and Bqt4
85 localize at the INM (Chikashige et al., 2009). Bqt3 and Bqt4 are required for anchoring
86 telomeres to the NE during vegetative growth and clustering telomeres to the spindle pole
87 body through the meiosis-specific telomere-binding proteins Bqt1 and Bqt2 (Chikashige et
88 al., 2006; Chikashige et al., 2009). Importantly, Bqt4 interacts with Lem2 (Hirano et al.,
89 2018), and the depletion of Bqt4 is synthetic-lethal with the depletion of Lem2 (Tange et al.,
90 2016; Kinugasa et al., 2019). Therefore, Bqt4 may play an important role in cell viability.
91 However, the non-telomeric vital roles of Bqt4 and the mechanisms underlying its
92 degradation remain unknown. In this study, we identified the factors required for Bqt4
93 degradation through an INM-associated degradation mechanism. We also demonstrated that

94 excess amounts of Bqt4 resulted in impaired nuclear morphology and growth defects,
95 indicating the importance of regulated degradation of Bqt4 for membrane homeostasis.
96
97 **Results**
98 **INM protein Bqt4 is degraded via the UPS**
99 Because the UPS accounts for the selective degradation of many proteins in the nucleus
100 (Enam et al., 2018; Franić et al., 2021), we first tested the requirement of the proteasome for
101 Bqt4 degradation. We treated cells expressing N-terminally GFP-tagged Bqt4 (GFP-Bqt4)
102 under its own promoter with bortezomib (BZ), a chemical proteasome inhibitor working in *S.*
103 *pombe* (Takeda et al., 2011), and assessed the fluorescence levels of GFP-Bqt4 at 4 h after
104 drug addition in the presence or absence of Bqt3. As a result of the treatment, GFP-Bqt4
105 fluorescence in the nuclei of both *bqt3*$^{+}$ and *bqt3*Δ cells was elevated (Fig. 1A). To confirm
106 this result, we measured protein levels by western blotting, which consistently showed an
107 increase in GFP-Bqt4 protein levels in these strains upon proteasomal inhibition by BZ (Fig.
108 1B). Notably, the GFP-Bqt4 signal was restored upon proteasome inhibition in the absence of
109 Bqt3 and also elevated in the presence of Bqt3. This suggests that Bqt4 is constitutively
110 turned over by the proteasome system and its association with Bqt3 antagonizes this process.
111 We sought to confirm this phenomenon by introducing temperature-sensitive *mts2-1* and
112 *mts3-1* proteasome mutations (Gordon and McGurk, 1993; Gordon et al., 1996). Using both
113 fluorescence microscopy and western blotting, we found that GFP-Bqt4 levels were increased
114 in *bqt3*$^{+}$ and *bqt3Δ* cells carrying these proteasome mutations at a restrictive temperature of
115 36 °C, as compared to the corresponding wild-type strains (Fig. 1C, D; Fig. S1). These results
116 indicate that Bqt4 degradation proceeds via the proteasome system.
117 Since proteins are ubiquitinated as a requirement for recognition by the proteasome,
118 we examined whether Bqt4 was modified by polyubiquitination. We immunoprecipitated

119 GFP-Bqt4 under denaturing conditions and detected associated ubiquitin by immunoblotting.
120 Ubiquitinated forms of Bqt4 were detected in *bqt3*Δ cells and were enriched in both *bqt3*$^{+}$
121 and *bqt3*Δ cells when proteasomal activity was inhibited (Fig. 1E), suggesting that Bqt4 was
122 targeted to the proteasome by polyubiquitin modification.
123 Bqt4 is degraded via the UPS in the absence of Bqt3, suggesting that Bqt3 plays a role
124 in stabilizing Bqt4 by protecting Bqt4 from degradation. To assess whether Bqt3 stabilizes
125 Bqt4, we determined the degradation kinetics of GFP-Bqt4 in the presence or absence of
126 Bqt3 by cycloheximide chase assay followed by western blotting. The result showed that
127 GFP-Bqt4 degraded faster in the absence of Bqt3 than in the presence of Bqt3 (Fig. 1F). This
128 indicates that Bqt4 is protected from proteasome-dependent degradation by Bqt3. Thus, Bqt4
129 is maintained at the INM by associating with Bqt3, and is polyubiquitinated and degraded
130 quickly once it dissociates from Bqt3.
131 Vacuolar autophagy is another pathway through which cells degrade proteins. Thus,
132 we next examined whether Bqt4 degradation is regulated by the vacuolar autophagy pathway
133 by analyzing GFP-Bqt4 levels in *bqt3*Δ cells lacking *isp6*$^{+}$ and *atg1*$^{+}$ genes. Isp6 is a serine
134 protease necessary for vacuolar function, and Atg1 is a serine/threonine protein kinase that is
135 the upstream initiator of the autophagy machinery. Deletion of these two genes has been
136 shown to completely impair the vacuolar autophagy pathway (Kohda et al., 2007). We found
137 that the deletion of *isp6* and *atg1* had no detectable effect on the quantity of GFP-Bqt4 in the
138 absence of Bqt3, suggesting that Bqt4 degradation does not involve the vacuolar autophagy
139 system (Fig. 1F). Collectively, we conclude that the Bqt4 protein is degraded by the UPS
140 without the involvement of the vacuolar autophagy pathway.
141
142 **Bqt4 degradation occurs in the nucleus**

143 Next, we determined whether Bqt4 was degraded in the nucleus by the nuclear proteasome.
144 In *S. pombe*, proper targeting of proteasomes to the nucleus requires the tethering factor, Cut8
145 (Tatebe and Yanagida, 2000). In *cut8* mutants, proteasomes fail to localize to the nucleus and
146 are mostly cytoplasmic (Tatebe and Yanagida, 2000). Because nuclear protein degradation
147 depends on the localization of proteasomes in the nucleus (Takeda and Yanagida, 2005), we
148 examined the levels of GFP-Bqt4 in *bqt3*$^{+}$ and *bqt3Δ* cells carrying the temperature-sensitive
149 *cut8-563* mutation. We found that GFP-Bqt4 degradation was suppressed in *cut8-563* cells
150 shifted to the nonpermissive temperature of 36°C (Fig. 2A, B). Taken together, our results
151 strongly suggest that Bqt4 is degraded mainly by the proteasome within the nucleus.
152
153 **Bqt4 degradation involves the Doa10 E3 ligase complex**
154 We next sought to identify the specific E3 ubiquitin ligase that directly recognizes Bqt4. As
155 Bqt4 is a protein associated with the INM, we investigated whether membrane-localized
156 Hrd1 and Doa10 E3 ligases participate in the Bqt4 degradation pathway. Deletion of *doa10*$^{+}$
157 partially restored GFP-Bqt4 levels in the absence of Bqt3, whereas deletion of *hrd1*$^{+}$ did not
158 (Fig. 3A and B, comparing *hrd1*Δ to *doa10*Δ). These results are consistent with previous
159 studies that showed that Doa10 partially localizes to the INM and is involved in the
160 degradation of certain nuclear and INM substrates, whereas Hrd1 is found exclusively in the
161 ER (Deng and Hochstrasser, 2006; Boban et al., 2014). Additionally, the double deletion of
162 *doa10*$^{+}$ and *hrd1*$^{+}$ showed no obvious synthetic effect on GFP-Bqt4 restoration compared
163 with the deletion of *doa10*$^{+}$ alone (Fig. 3A, B). We also measured the amount of GFP-Bqt4 in
164 mutants lacking Ubc6 and Ubc7, which are E2 ubiquitin-conjugating enzymes associated
165 with Doa10 (Swanson et al., 2001). We found that GFP-Bqt4 levels increased to some extent
166 in *ubc6*Δ, *ubc7*Δ single, and *ubc6*Δ *ubc7*Δ double mutants (Fig. 3C, D). These findings
167 indicate that the Doa10 complex contributed to the degradation of Bqt4 in the INM.

168 Although degradation of Bqt4 depended on Doa10, the level of GFP-Bqt4 was only
169 partially restored in the *doa10*Δ mutant (Fig. 3A, B). Therefore, we attempted to identify
170 other redundant E3 ligases involved in Bqt4 degradation. We constructed mutants of E3
171 ligases and their components that have been suggested to localize to or function in the ER
172 and nucleus, namely *meu34*Δ, *dsc1*Δ, *ubr1*Δ, *ubr11*Δ, *san1*Δ, *hul5*Δ, *ptr1-1*, and *cut9-665*
173 (PomBase (https://www.pombase.org), Matsuyama et al., 2006, Nielsen et al., 2014; Enam et
174 al., 2018; Franić et al., 2021), and observed GFP-Bqt4 fluorescence intensity in these
175 mutants. The mutants tested showed no detectable increase in fluorescence, except for the
176 *hul5*Δ mutant (Fig. S2). The *hul5*Δ cells showed a slight increase in the fluorescence level of
177 GFP-Bqt4, but showed no increase in GFP-Bqt4 level in western blotting (Fig. S3). Instead, a
178 small degraded fragment was observed (Fig. S3), suggesting that the increase in the GFP
179 signal in *hul5*Δ cells reflects this degraded product. Therefore, Doa10 is the only E3 ligase
180 identified to date that ubiquitinates Bqt4.
181
182 **Bqt4 is an integral membrane protein**
183 We have previously shown that Bqt4 localizes exclusively to the nucleoplasmic side of the
184 INM, and this localization requires its C-terminal helix (Chikashige et al., 2009). However,
185 this C-terminal helix was predicted to be a weak candidate for TMD (Fig. S4), we examined
186 whether Bqt4 is an integral or peripheral membrane protein to understand how Bqt4 is
187 removed from INM before degradation. Therefore, we performed membrane protein
188 extraction experiments. In brief, the membrane fraction was isolated from the cell extract,
189 treated under various conditions, and then separated into pellet and supernatant fractions by
190 ultracentrifugation, followed by western blotting; a protein was expected to enter the pellet
191 fraction if it remained in the lumen or associated with the membrane after the treatment.
192 GFP-ADEL (Pidoux & Armstrong, 1992) and Ish1-GFP were used as controls for the luminal

193 and integral membrane proteins, respectively. As shown in Fig. 4A, all these proteins were
194 extracted from the membrane by treatment with Triton X-100 and 0.5 M NaCl. However,
195 similar to Ish1, Bqt4 did not dissociate from the membrane by sodium carbonate (pH 11.5) or
196 urea, which can strip peripheral membrane proteins. In contrast, GFP-ADEL was released
197 from the membrane following sodium carbonate treatment, as expected for luminal proteins.
198 Thus, Bqt4 is likely to behave as a tail-anchored protein integrally embedded in the INM in
199 the presence of Bqt3.
200 To further characterize the properties of TMD, we examined whether Bqt4 behaves as
201 an integral membrane protein in the absence of Bqt3 using a membrane extraction assay. As
202 most of Bqt4 protein is degraded in the *bqt3*Δ cells, we used the *bqt3*Δ*doa10*Δ cells to
203 prevent the degradation. Bqt4 was extracted from the membrane by detergent, but not by
204 sodium carbonate and urea (Figure 4B), as was the case in the *bqt3*$^{+}$ condition, indicating that
205 the TMD of Bqt4 was embedded in the INM independent of Bqt3.
206
207 **Degradation of Bqt4 requires the Cdc48 retrotranslocation complex**
208 The ATPase Cdc48 has been shown to facilitate the degradation of ubiquitinated ERAD
209 membrane substrates by extracting them from the ER membrane in *S. cerevisiae* cells (Ye et
210 al., 2001; Jarosch et al., 2002; Rabinovich et al., 2002; Wolf and Stolz, 2012). Therefore, we
211 investigated whether Cdc48 is necessary for Bqt4 degradation. To this end, we generated a
212 *cdc48* mutant bearing mutations in both the D1 (P267L) and D2 (A550T) ATPase domains
213 based on the temperature-sensitive *cdc48-6* allele in *S. cerevisiae* (Schuberth and Buchberger,
214 2005; Ruggiano et al., 2016) (Fig. 5A). The *cdc48* mutant (*cdc48-P267L/A550T*) exhibited
215 cold-sensitive growth defects (Fig. 5B), suggesting that these mutations impaired Cdc48
216 activity in *S. pombe*. Inactivation of *cdc48-P267L/A550T* by shifting to a nonpermissive
217 temperature of 16°C elevated the level of GFP-Bqt4 in *bqt3*$^{+}$ and *bqt3*Δ cells, as observed

218 under fluorescence microscopy (Fig. 5C) and western blotting (Fig. 5D); however, it was
219 degraded at 33°C (Fig. S5), indicating that Cdc48 was required for Bqt4 degradation.
220
221 **The C-terminal TMD of Bqt4 acts as a degradation signal**
222 We previously showed that Bqt4 degradation depends on its C-terminal TMD (residues 414-
223 432) (Chikashige et al., 2009). To identify the minimal region of Bqt4 that is sufficient for its
224 degradation, we analyzed truncated C-terminal fragments based on the structure of Bqt4
225 predicted by AlphaFold2 (Fig. 6A, Fig. S6). The Bqt4 fragment containing the helix domain
226 and the adjacent intrinsically disordered sequence (Bqt4C$^{369-432}$) reproduced the behavior of
227 full-length Bqt4, as shown in Fig. 1A, that is, localization to the NE and responses to BZ,
228 both in the presence and absence of Bqt3 (Fig. 6A, Bqt4C$^{369-432}$). The helix domain alone
229 (Bqt4C$^{394-432}$) showed weaker localization to the NE and was somewhat diffused to the
230 membrane compartments in the cytoplasm; nevertheless, this fragment was degraded in the
231 absence of Bqt3, and its level increased with BZ treatment (Fig. 6A, Bqt4C$^{394-432}$). The TMD
232 alone (Bqt4C$^{414-432}$) showed even weaker localization at the NE with diffusion to the
233 cytoplasm, but showed the same responses, that is, degradation in the absence of Bqt3 and
234 increased levels upon BZ treatment (Fig. 6A, Bqt4C$^{414-432}$). These results indicate that the C-
235 terminal fragment containing residues 369–432 was necessary and sufficient for the NE
236 localization of Bqt4, and its truncation successively reduced NE localization. These results
237 also indicate that the C-terminal TMD of Bqt4 is sufficient for its proteasome-mediated
238 degradation.
239 To further narrow down the TMD of Bqt4 for proteasome-dependent degradation and
240 Bqt3-dependent protection against degradation, we generated constructs containing a shorter
241 TMD with the last seven residues truncated (Bqt4C$^{369-425}$). The fragment Bqt4C$^{369-425}$ lost its
242 dependency on Bqt3 for degradation and exhibited similar behaviors in the presence or

243 absence of Bqt3 (Fig. 6A, Bqt4C$^{369-425}$): this fragment showed increased signal levels in the
244 presence of BZ, indicating that it is also a substrate of proteasomal degradation in a Bqt3-
245 independent manner. As the level of Bqt4C$^{369-425}$ were not restored by *doa10* deletion, the
246 fragment is likely degraded by a distinct pathway from Doa10 (Supplementary Fig. S7). To
247 further characterize the reason why these fragments were degraded independent of Bqt3, we
248 examined the interaction between these fragments and Bqt3 as well as the membrane
249 association state of these fragments. The results of the yeast-two-hybrid (Y2H) assay showed
250 that the fragments lacking the last seven residues did not bind to Bqt3 (Fig. 6B). In addition,
251 Bqt4C$^{369-425}$ was partially extracted by sodium carbonate (Fig. 6C), suggesting that the last
252 seven residues assisted the membrane-embedding ability of the TMD. Thus, we concluded
253 that the entire TMD (414–432) is the minimal region of the Bqt3-binding site and is a degron
254 for proteasome-dependent degradation that is protected by Bqt3 (Fig. 6D).
255
256 **Excess Bqt4 causes deformation of the NE**
257 We observed that inhibition of proteasomal degradation caused striking NE expansion and
258 deformation, with irregular protrusions and invaginations, especially in *bqt3*$^{+}$ cells, in which
259 Bqt4 levels were excessively high (Fig. 1A, C). We hypothesized that high levels of Bqt4 in
260 these cells were responsible for this abnormal NE morphology. To test this possibility, we
261 inhibited proteasomal degradation in the presence or absence of endogenous Bqt4 and
262 visualized the NE using Ish1-GFP as an NE marker, and then nuclear deformation was
263 assessed by measuring the roundness of the nucleus. Only when Bqt4 was present, a strong
264 deformation of the NE was observed upon proteasomal inhibition (see *bqt4*$^{+}$+BZ; Fig. 7A),
265 suggesting that Bqt4 was an essential factor causing this phenomenon. To ascertain whether
266 this abnormal phenotype was caused by an accumulation of Bqt4, we overexpressed GFP-
267 Bqt4 under the *nmt1* promoter using YAM2 to control the expression level. YAM2, a

268 chemical compound, suppresses *nmt1* promoter activity depending on its concentration
269 (Nakamura et al., 2011). Overexpression of GFP-Bqt4 reproduced the nuclear-deformed
270 morphology (Fig. 7B), and NE proliferation and deformation became more striking in cells
271 that expressed higher levels of GFP-Bqt4 (Fig. 7C, D), indicating that the abnormal NE
272 morphology depended on the amount of Bqt4. Taken together, these results support our
273 hypothesis that Bqt4 is the only protein whose accumulation upon inhibition of degradation
274 induces aberrant nuclear morphology. Finally, we investigated whether an excess of GFP-
275 Bqt4 was toxic. We found that overproduction of GFP-Bqt4 caused a growth defect in both
276 *bqt3*$^{+}$ and *bqt3Δ* strains compared to cells expressing endogenous levels of Bqt4 (Fig. 7E).
277 Altogether, these observations suggest that Bqt4 plays an important role in regulating NE
278 morphology, and a nuclear proteasomal degradation pathway controlling the quantity of Bqt4
279 is crucial for nuclear membrane homeostasis.
280

281 **Discussion**

282 In this study, we identified the molecular factors required for the degradation of the INM
283 integral protein Bqt4 in *S. pombe* (Fig. 8). Bqt4 is ubiquitinated and degraded by the nuclear
284 proteasome via an INMAD mechanism involving the Doa10 E3 ligase, which possibly
285 recognizes the C-terminal TMD of Bqt4 as a degron. In addition, the AAA-ATPase Cdc48 is
286 required for Bqt4 degradation. We also demonstrated that the accumulation of undegraded
287 Bqt4 in the INM caused strong deformation of the NE and resulted in growth defects. Bqt4
288 escapes degradation by interacting with Bqt3 through its C-terminal TMD. Excess amounts
289 of Bqt4 that were not bound to Bqt3 were subjected to INMAD-mediated degradation to
290 avoid the accumulation of Bqt4 at the NE. These findings contribute to our understanding of
291 the significance of INM protein degradation in INM homeostasis.

292

293 **Bqt4 is a native INM degradation substrate containing an intramembrane degron**

294 Studies on mammalian cells have suggested that integral INM proteins are largely stable
295 (Toyama et al., 2013; Buchwalter et al., 2019); however, it has been difficult to study their
296 turnover. In the budding yeast *S. cerevisiae*, most of the INMAD substrates characterized
297 thus far are not native INM proteins, but rather nuclear soluble proteins (Swanson et al.,
298 2001; Ravid et al., 2006) and ER membrane proteins that are unassembled or mislocalized to
299 the INM (Foresti et al., 2014; Khmelinskii et al., 2014; Natarajan et al., 2020). Thus, our
300 study on Bqt4 provides an opportunity for a native INM substrate to obtain further insight
301 into the mechanisms governing INM protein degradation. In addition to several previous
302 studies that reported a handful of native INM substrates (Boban et al., 2014; Pantazopoulou
303 et al., 2016; Smoyer et al., 2019; Koch et al., 2019), our results on the degradation of the
304 INM protein Bqt4 demonstrate that INMAD is responsible for not only maintaining INM

305 identity by removing foreign proteins but also for maintaining the proteostasis of INM
306 integral components.
307 An important question is whether INMAD machinery specifically recognizes its
308 substrates. Although a degradation signal has yet to be identified for integral INM substrates
309 of INM-localized E3 ubiquitin ligases, such as Doa10 and the Asi complex, we identified that
310 Bqt4 has an intramembrane degron. This suggests that INMAD may not simply detect and
311 degrade misfolded or mislocalized proteins in the INM, but instead specifically recognizes a
312 substrate to regulate its protein levels.
313
314 **An INM protein degradation pathway in *S. pombe***
315 In *S. cerevisiae*, the Doa10 E3 ubiquitin ligase cooperates with the Asi complex in INMAD
316 (Koch and Yu, 2019; Smoyer and Jaspersen, 2019; Mannino and Lusk, 2022). As homologs
317 of Asi proteins are absent in *S. pombe* as in other species, INMAD mechanisms may be
318 diverse among organisms. However, increasing evidence has shown that the degradation of
319 INM proteins in plants and mammals also employs the UPS and Cdc48/p97 (Tsai et al., 2016;
320 Huang et al., 2020; Krshnan et al., 2022), suggesting a general mechanism for INM protein
321 degradation.
322 In *S. cerevisiae*, Doa10 E3 ligase can passively diffuse from the ER to the INM and
323 functions in both ERAD and INMAD (Deng and Hochstrasser, 2006). In particular, Doa10
324 has been implicated in mediating the degradation of the INM protein Asi2, which is a
325 component of INMAD (Boban et al., 2014). In *S. pombe*, Bqt4 degradation also depends on
326 Doa10, indicating that Bqt4 is subject to regulation by INMAD. In addition, our data indicate
327 that *S. pombe* might possess additional unidentified redundant E3 ligases cooperating with
328 Doa10 at the INM. Because Bqt4 is supposed to be recognized by these E3 ligases at its
329 transmembrane degron, it is expected that the unidentified E3 ligases also localize to the INM

330 ("X(E3)" in Fig. 8). Similar situations in which unidentified E3 ligases degrade an INM
331 substrate have been reported in *S. cerevisiae* (Pantazopoulou et al. 2016). Similarly, INM-
332 localized E3 ligases have yet to be identified in higher eukaryotes. We speculate that the
333 uncharacterized E3 ligases functioning at the INM in *S. pombe* might operate with E2
334 ubiquitin-conjugating enzymes other than Ubc6 and Ubc7, because degradation of Bqt4
335 exhibits limited dependence on these enzymes. Thus, it would be of great interest to identify
336 and characterize other membrane-associated E3 ligases and E2 conjugating enzymes that
337 mediate protein degradation at the INM.
338 The Cdc48 complex plays a central role in the ERAD degradation of ER integral
339 membrane proteins by exerting a pulling force on the ubiquitinated membrane protein via its
340 ATPase activity (Braun, 2002; Rabinovich et al., 2002; Wolf and Stolz, 2012; Bodnar and
341 Rapoport, 2017). Cdc48 has also been implicated in the degradation of INM proteins Asi1
342 and Msp3 in *S. cerevisiae* (Pantazopoulou et al. 2016; Koch et al., 2019). In *S. pombe*, Cdc48
343 mutations at its ATPase active center impair Bqt4 degradation (Fig. 5), indicating that
344 ERAD/INMAD degradation involves the Cdc48 complex; however, it remains unclear
345 whether Cdc48 extracts Bqt4 from the INM.
346
347 **The biological significance of Bqt4 degradation**
348 The INM protein Bqt4 has been suggested to have non-telomeric functions that are currently
349 unknown but are vital for cell growth, as the double deletion of Bqt4 and Lem2 results in
350 synthetic lethality (Tange et al., 2016; Hirano et al., 2018; Kinugasa et al., 2019; Hirano et
351 al., 2023b). In cells lacking both Bqt4 and Lem2, nuclear envelope rupture occurs in
352 association with leakage of nuclear proteins into the cytoplasm, suggesting that Bqt4, in
353 cooperation with Lem2, plays an essential role in maintaining nuclear membrane integrity
354 (Kinugasa et al., 2019). The nuclear membrane rupture phenotype can be rescued by the

355 increased expression of Elo2, a fatty acid elongase that catalyzes the synthesis of very-long-
356 chain fatty acids (Kinugasa et al., 2019), and Tlc4, a ceramide synthase homolog which is
357 localized in the Golgi (Hirano et al., 2023b). In addition, the depletion of Bqt4 and Lem2
358 leads to a reduction in the quantity of t20:0/24:0 phytoceramide, the most abundant ceramide
359 species in *S. pombe*, and this reduction can be prevented by the overexpression of these
360 proteins (Kinugasa et al., 2019; Hirano et al., 2023b). These findings strongly suggest that
361 Bqt4 is involved in nuclear membrane lipid metabolism. Thus, we propose that the abnormal
362 accumulation of Bqt4 at the INM may result in excessive lipid synthesis, ultimately leading
363 to nuclear membrane expansion and deformation. One possibility is that Bqt4 promotes the
364 synthesis of phospholipids, a major component of the nuclear membrane, as Bqt4 binds to an
365 enzyme involved in lipid synthesis (Hirano et al, 2023a). Several lines of evidence suggest
366 that increased phospholipid synthesis from phosphatidic acid induces striking NE membrane
367 deformation (Santos-Rosa et al., 2005; Barbosa et al., 2015). The exact mechanisms leading
368 to the deformed nuclear morphology upon the accumulation of Bqt4 remain to be elucidated.
369 Further investigations will advance our understanding of the role of INM protein degradation
370 in the maintenance of nuclear membrane homeostasis.
371
372

373 **Materials and methods**

374 **Yeast strains and culture media**

375 All *S. pombe* strains used in this study are listed in Table S1. Unless otherwise specified, all
376 *S. pombe* strains were cultured in yeast extract with supplements (YES) medium. Malt extract
377 medium (ME) was used to induce sporulation. G418 disulfate (Nacalai Tesque, Japan),
378 hygromycin B (Wako, Japan), nourseothricin sulfate (Werner BioAgents, Germany), and
379 blasticidin S (Wako, Japan) were used at concentrations of 100, 200, 100, and 100 μg/ml,
380 respectively, to select strains bearing the respective selection marker.

381

382 **Construction of plasmids and strains**

383 All plasmids were constructed using the NEBuilder system (New England BioLabs, MA,
384 USA) and enzymatic digestion and ligation (TaKaRa, Japan) systems, according to the
385 manufacturer's instructions. Gene disruption and GFP tagging were performed using the
386 direct chromosomal integration method (Wach, 1996; Bähler et al., 1998). The integration
387 cassettes were amplified using a two-step PCR. In the first PCR, fragments (~500 bp
388 genomic regions upstream and downstream of the gene of interest) were amplified from the
389 wild-type *S. pombe* genome using KOD One DNA polymerase (TaKaRa Bio Inc., Japan).
390 The first PCR products were used as primers in the second PCR step to amplify a cassette for
391 integration, which contained a selection marker. For gene disruption, pFA6-kanMX6 (Bähler
392 et al., 1998), pCR2.1-hph, pCR2.1-bsd, and pCR2.1-nat (Sato et al., 2005) were used to
393 generate the integration cassettes. For GFP tagging, pFA6-GFP(S65T)-kanMX6 (Bähler et
394 al., 1998) was used to generate the GFP-containing integration cassettes. The cassettes were
395 then transformed into *S. pombe* cells and the desired integrant strains were selected on YES
396 plates containing the appropriate selection agent. Correct disruption and integration were
397 confirmed by genomic PCR at the 5′ and 3′ ends using KOD FX Neo (TaKaRa Bio Inc.,

398 Japan). We confirmed that N-terminally GFP-tagged Bqt4 is functional, as it suppressed the
399 synthetic lethality of *bqt4* and *lem2* double deletion (Tange et al., 2016) and anchored
400 telomeres to the NE (Chikashige et al., 2009).
401
402 **Fluorescence microscopy**
403 All fluorescence microscopy images were obtained from live cells. Fluorescence microscopy
404 data of intracellular GFP fusion proteins were collected using a DeltaVision microscope
405 system (GE Healthcare Inc., USA) equipped with a pco.edge 4.2 sCMOS camera (PCO,
406 Germany) and a ×60 PlanApo N OSC oil-immersion objective lens (numerical aperture
407 NA=1.4, Olympus, Japan). Cells were precultured from fresh colonies and cultured in YES
408 medium at 30°C to reach the logarithmic growth phase (5–10×10^6 cells/ml). The cells were
409 then attached to glass-bottomed culture dishes coated with soybean lectin (Sigma-Aldrich,
410 USA), covered with Edinburgh minimal medium with glutamate (EMMG) medium, and
411 observed at specified temperatures.
412
413 **Image quantification and processing**
414 An identical fluorescence intensity range was applied to all images presented in each panel
415 using the Fiji software (Schindelin et al., 2012).
416 To quantify the fluorescence intensity in the nucleus, we used the Fiji software. First,
417 we generated the sum projection image from the raw z-stack images and then subtracted the
418 background signal from the entire image by measuring the mean intensity of a region where
419 no cells were present. Second, the nuclear region was selected manually or semi-
420 automatically. For semi-automatic selection, individual nuclei were selected (original image),
421 and the selected image was blurred using Gaussian blur (blurred image). An appropriate
422 sigma value was applied depending on the image contrast. An edge-enhanced image was

423 generated by subtracting the blurred image from the original image. A threshold was applied
424 to the nuclear region using the appropriate minimum and maximum intensity ranges. Third,
425 the threshold region was applied to the original image and the total fluorescence intensity of
426 the region was quantified. The nuclear intensities obtained from *bqt3*$^{+}$ cells were averaged
427 and the values were used to calculate the relative fluorescence intensity. The relative
428 fluorescence intensities were plotted, and the results are presented as the mean ± standard
429 deviation.

430 For the roundness index measurement, after selecting individual nuclei, a threshold
431 was applied to the nuclear membrane signal using the appropriate fluorescence intensity
432 ranges. The nuclear region was filled in, and the roundness index was measured using the
433 built-in function in Fiji.

434

435 **Western blotting**

436 Cells were precultured in YES medium at 30°C overnight, inoculated in fresh YES, and then
437 cultured until the cell concentration reached mid-log phase (5–10×10^6 cells/ml).
438 Approximately 5×10^7 cells were harvested by centrifugation at 4°C, and the cell pellet was
439 washed with 1 ml ice-cold water containing 1 mM phenylmethylsulfonyl fluoride (PMSF).
440 The cells were lysed in 150 µl of ice-cold 1.85 M NaOH containing 7.5% β-mercaptoethanol
441 (β-ME) on ice for 15 min, followed by the addition of 150 µl of ice-cold 55% (v/v)
442 trichloroacetic acid (TCA) to precipitate the proteins, incubation on ice for 15 min, and
443 centrifugation (10 min, 14,000 ×g, 4°C). The protein pellet was then washed twice with ice-
444 cold acetone and dissolved in sample solubilization buffer [50 mM Tris-HCl (pH 8.0), 1%
445 SDS, 1× protease inhibitor cocktail (P8215, Sigma-Aldrich, USA), 1 mM PMSF, and 1 mM
446 bortezomib]. Total protein concentrations were determined using the BCA assay (Thermo
447 Fisher Scientific, USA) according to the manufacturer's protocol. The samples were further

448 diluted in 2× Laemmli SDS sample buffer to a concentration of 1 μg/μl. After the addition of
449 dithiothreitol to a concentration of 50 mM, the samples were heated at 95°C for 10 min
450 before immunoblotting. Identical amounts of protein (10 μg) were separated by SDS–PAGE
451 and transferred to a polyvinylidene difluoride membrane. The membranes were blocked for 1
452 h at room temperature (approximately 26–28°C) in blocking solution [PBST (10 mM
453 Na_2HPO_4, 137 mM NaCl, 2.7 mM KCl, 1.76 mM KH_2PO_4, and 0.1% Tween 20) containing
454 5% skim milk (Nacalai Tesque, Japan)]. To detect the GFP fusion proteins and β-actin as a
455 loading control, the membranes were probed with anti-GFP rabbit polyclonal antibody
456 (Rockland, USA; 1:2,000 dilution) or anti-β-actin mouse monoclonal antibody (Abcam, UK;
457 1:2,000 dilution) in blocking solution overnight at 4°C. After three rounds of washing with
458 PBST, the membranes were incubated with appropriate horseradish peroxidase-conjugated
459 secondary antibodies (1:2,000 dilution, Cytiva, USA) in a blocking solution at room
460 temperature for 2 h. After three rounds of washing with PBST, the immunoreactive bands
461 were detected using a chemiluminescence system (ImmunoStar LD; Wako, Japan) on a
462 ChemiDoc imaging system (Bio-Rad, USA).
463
464 **Proteasome inhibition**
465 Cells were grown in YES medium until early mid-log phase (2–5×10^6 cells/ml), as described
466 above. The culture was then divided into two groups, and the proteasome inhibitor
467 bortezomib (LC Laboratories, USA) dissolved in dimethyl sulfoxide (DMSO) was added to
468 one culture to a final concentration of 1 mM; the same amount of DMSO was added to the
469 other culture. The cells were incubated at 26°C for 4 h before harvesting for fluorescence
470 microscopy and immunoblotting.
471
472 **Temperature-sensitive mutant experiments**

473 For the temperature-sensitive mutant experiments, cells harboring *ts* or *cs* mutations were
474 grown in YES medium until the early mid-log phase (2–5×10^6 cells/ml) at 26°C and 33°C,
475 respectively. The culture temperature was shifted up to 36°C or down to 16°C, and then the
476 cells were incubated for 4 h and 15 h, respectively, before harvesting.
477
478 **Ubiquitination detection assay**
479 The ubiquitination detection assay was performed as described previously (Boban et al.,
480 2014) with modifications. Cells were grown in YES medium at 30°C until the mid-log phase
481 (5–10×10^6 cells/ml), and approximately 5×10^8 cells were harvested by centrifugation at 4°C.
482 Where indicated, the proteasome inhibitor bortezomib was added at a final concentration of 1
483 mM for 4 h before the cells were collected. The same volume of DMSO was added to the
484 control samples. The cells were washed with cold water containing 1 mM PMSF and lysed in
485 250 µl of 1.85 N NaOH solution containing 7.5% β-ME for 15 min on ice. Subsequently, the
486 proteins were precipitated by adding 250 µl of 55% (v/v) TCA, followed by incubation for 15
487 min on ice. The proteins were pelleted by centrifugation (10 min, 14,000 ×g, 4°C) and
488 washed with 500 µl of 50 mM Tris before being dissolved in 200 µl denaturation solution [25
489 mM Tris-HCl pH 7.4, 2% SDS, 2 mM ethylenediaminetetraacetic acid (EDTA), 1× protease
490 inhibitor cocktail (P8215, Sigma-Aldrich, USA), 1 mM PMSF, 1 mM bortezomib, 10 µM
491 PR-619 (SML0430, Sigma-Aldrich, USA), and 50 mM 2-chloroacetamide (032-09762, Fuji
492 film Wako, Japan)]. Total protein concentrations were determined using the BCA assay
493 (Thermo Fisher Scientific, USA) according to the manufacturer's protocol. The samples were
494 incubated at 65°C for 10 min and clarified by centrifugation (5 min, 15,000 ×g, room
495 temperature). Equal amounts of protein lysates were diluted five-fold with cold IP dilution
496 buffer (50 mM Tris-HCl pH 7.5, 1.2% Triton X-100, 2 mM EDTA, 100 mM NaCl, 1 ×
497 protease inhibitor cocktail, 1 mM PMSF, 1 mM bortezomib, 10 µM PR-619, and 50 mM 2-

498 chloroacetamide), incubated with gentle rotation at 4°C for 1 h, and cleared by centrifugation
499 at 14,000 ×g for 10 min. A portion (20 µl) of the sample (2% input) was mixed with 2×
500 Laemmli SDS sample buffer (20 µl) and frozen until analysis. The remaining sample was
501 mixed with antibody-coupled beads prepared from 2 µg anti-GFP rabbit polyclonal antibody
502 (Rockland) and 50 µl protein-A-coupled dynabeads (Life Technologies, USA), according to
503 the manufacturer's instructions. The samples were immunoprecipitated at 4°C for 3 h with
504 gentle rotation, and then pelleted using a magnet. The pellets were then washed as follows:
505 twice with washing solution A (50 mM Tris-HCl pH 7.4, 2 mM EDTA, 100 mM NaCl, 1%
506 Triton X-100, 0.4% SDS), once with washing solution B (50 mM Tris-HCl pH 7.4, 2 mM
507 EDTA, 350 mM NaCl, 1% Triton X-100) including a 10-min incubation at 4°C with gentle
508 rotation, and finally once with washing solution A. To elute the immunoprecipitated protein,
509 50 µl of 1× Laemmli SDS sample buffer was added to the pellet, and the mixture was
510 incubated for 10 min at 65°C. Ten microliters of each sample were separated on SDS-PAGE
511 gels (8%). For the analysis of immunoprecipitated GFP-Bqt4, the eluate was diluted 1:20
512 with 1× Laemmli SDS sample buffer. Immunoblotting was performed using an anti-GFP
513 mouse monoclonal antibody (JL8; 1:1000; TaKaRa Bio Inc.) and an anti-ubiquitin mouse
514 monoclonal antibody (P4D1, 1:1000; Santa Cruz Biotechnology, USA). Protein levels in the
515 input samples were assessed using an anti-β-actin antibody (1:2000; Abcam).
516
517 **Cycloheximide chase assay**
518 The *bqt3*$^{+}$ or *bqt3*Δ cells expressing GFP or GFP-Bqt4 were grown in YES medium to the
519 mid-log phase (approximately 5×10^{6} cells/ml). After adding final 200 µg/ml cycloheximide
520 (C7698, Sigma-Aldrich), the cells were cultured for 0, 5, 10, 30, and 60 min for protein
521 degradation. Immediately after culturing, stop solution (2 mM PMSF + 5× protease inhibitor
522 cocktail) was added to the cells, and the cells were placed on ice for 5 min. The cells were

523 harvested by centrifugation (8,000×g for 3 min) and subjected to western blotting as
524 described above.
525
526 **Membrane association assay**
527 The membrane association assay was performed according to a previously published protocol
528 (Habeck et al., 2015) with slight modifications. *S. pombe* cells expressing GFP-Bqt4 and
529 control proteins (Ish1-GFP and GFP-ADEL) were grown to the mid-log phase and mixed at
530 an appropriate ratio before cell harvesting by centrifugation at 4°C. The harvested cells
531 (~5×10^8 cells) were washed with cold water containing 1 mM PMSF and resuspended in 1 ml
532 cold fractionation buffer (FB; 0.7 M sorbitol, 50 mM Tris-HCl pH 7.4, 150 mM NaCl, 1×
533 protease inhibitor cocktail, 1mM PMSF, 1 mM bortezomib). Resuspended cells were lysed
534 using a bead shocker (2,700 rpm for 10 cycles of 60 s on and 60 s off; Yasui Kikai, Co.,
535 Japan), followed by washing the beads three times with 200 µl FB. The cell extracts were
536 combined, and cell debris and intact nuclei were removed by centrifugation (2000 ×g for 5
537 min at 4°C). Membrane fraction was isolated by ultracentrifugation at 100,000 ×g for 1 h at
538 4°C. The membrane was thoroughly resuspended in FB and divided into four separate
539 aliquots that were subjected to one of the following treatments: (1) FB alone; (2) 0.1 M
540 Na_2CO_3, pH 11.5; (3) 2.5 M urea; or (4) 1% Triton X-100 and 0.5 M NaCl. After incubation
541 for 1 h on ice with occasional mixing, the samples were separated into pellet (P) and
542 supernatant (S) fractions by ultracentrifugation at 100,000 ×g for 45 min at 4°C. The pellets
543 were washed once with appropriately supplemented FB by centrifugation (100,000 ×g for 45
544 min at 4°C) before being resuspended in FB. Proteins were then precipitated from the pellet
545 and supernatant fractions by adding TCA to a final concentration of 20% (v/v). After 30 min
546 of incubation on ice, the proteins were pelleted by centrifugation (16,000 ×g for 10 min at

547 4°C), washed twice with ice-cold acetone, and dissolved in 1× Laemmli SDS sample buffer.
548 Samples were incubated for 10 min at 95°C before immunoblotting.
549
550 **Yeast two-hybrid assay**
551 The yeast two-hybrid assay was performed as described in our previous paper, with slight
552 modifications (Asakawa et al., 2022). GFP-Bqt4 fragments and Bqt3 were expressed from
553 pGADT7 and pGBKT7 plasmids in the budding yeast strain (AH109). To examine protein
554 interactions, suspensions of the transformants were spotted onto SD plates with dropout
555 supplements: Leu/-Trp (cat #630417) or -Ade/-His/-Leu/-Trp (cat #630428) (Takara Bio).
556 The strains used in this assay are listed in Table S1.
557
558 **Spot assay**
559 Cells expressing GFP-Bqt4 under the control (*bqt4p*) or nmt1 promoter (*nmt1p*) were pre-
560 cultured in YES medium overnight. Five-fold dilution series of the cells (starting
561 concentration was 8.0×10^5 /mL) were spotted on the EMMG medium plates supplemented
562 with or without 10 μM thiamine, and then the plates were incubated at 30°C for 4 days.
563 For the temperature-sensitivity growth assay, wild-type and Cdc48 mutant cells were
564 spotted in a five-fold dilution series and incubated at 16, 20, 26, 30, 33, and 37°C for 3–6
565 days.
566
567 **Acknowledgements**
568 We thank Chizuru Ohtsuki and Yoshino Kubota for their technical assistance; We also thank
569 to Professor Mitsuhiro Yanagida (OIST) and the National BioResource Project Yeast in Japan
570 for providing the *S. pombe* strains.
571

Competing interests

The authors declare no competing financial or non-financial interests.

Author contributions

Conceptualization: T.K.L., Y. Hirano, T.H., Y. Hiraoka; Methodology: T.K.L.,Y. Hirano, H.A., K.O., T.H., Y. Hiraoka; Validation: T.K.L, Y. Hirano, K.O., T.H., Y. Hiraoka; Formal analysis: T.K.L, Y. Hirano; Investigation: T.K.L, Y. Hirano, H.A.; Resources: K.O, T.F, Y. Hiraoka; Data curation: T.K.L., Y. Hirano, H.A., K.O., T.F., T.H., Y. Hiraoka; Writing - original draft: T.K.L, Y. Hirano, T.H., Y. Hiraoka; Writing - review & editing: T.K.L., Y. Hirano, H.A., K.O., T.F., T.H., Y. Hiraoka; Visualization: T.K.L., Y. Hirano; Supervision: T.H., Y. Hiraoka; Project administration: Y. Hiraoka; Funding acquisition: Y. Hirano, K.O., T.F., T.H., Y. Hiraoka.

Funding

This study was supported by the Japan Society for the Promotion of Science (JSPS) KAKENHI grants JP20H05891 (to Y. Hirano), JP19H03222, JP20H05324 (to K.O.), JP18H05528 (to T.H.), JP20H00454, JP23K05636 (to Y. Hiraoka) and by a CREST grant from the Japan Science and Technology Agency (JPMJCR21E6) to T.F.

Data availability

Further information and requests for resources and reagents should be directed to Yasushi Hiraoka (hiraoka@fbs.osaka-u.ac.jp)

References

Asakawa, H., Hirano, Y., Shindo, T., Haraguchi, T., Hiraoka, Y. (2022). Fission yeast Ish1 and Les1 interact with each other in the lumen of the nuclear envelope. *Genes Cells* **27**, 643–656. doi: 10.1111/gtc.12981

Barbosa, A.D., Sembongi, H., Su, W.-M., Abreu, S., Reggiori, F., Carman, G.M., Siniossoglou, S. (2015). Lipid partitioning at the nuclear envelope controls membrane biogenesis. *Mol. Biol. Cell* **26**, 3641–3657. doi: 10.1091/mbc.E15-03-0173

Bähler, J., J.Q. Wu, M.S. Longtine, N.G. Shah, A. McKenzie, A.B. Steever, A. Wach, P. Philippsen, and J.R. Pringle. (1998). Heterologous modules for efficient and versatile PCR-based gene targeting in *Schizosaccharomyces pombe*. *Yeast*. 14, 943-951. doi: 10.1002/(SICI)1097-0061(199807)14:10<943::AID-YEA292>3.0.CO;2-Y

Boban, M., Pantazopoulou, M., Schick, A., Ljungdahl, P.O., Foisner, R. (2014). A nuclear ubiquitin-proteasomal pathway targets inner nuclear membrane protein Asi2 for degradation. *J. Cell Sci.* **127**, 3603-3613. doi: 10.1242/jcs.153163

Bodnar N.O., Rapoport T.A. (2017). Molecular Mechanism of Substrate Processing by the Cdc48 ATPase Complex. *Cell* **169**, 722-735. doi: 10.1016/j.cell.2017.04.020

Braun, S., Matuschewski, K., Rape, M., Thoms, S., Jentsch S. (2002). Role of the ubiquitin-selective $CDC48^{UFD1/NPL4}$ chaperone (segregase) in ERAD of OLE1 and other substrates. *EMBO J.* **15**, 615-621. doi: 10.1093/emboj/21.4.615

Buchwalter, A., Schulte, R., Tsai, H., Capitanio, J., Hetzer, M. (2019). Selective clearance of the inner nuclear membrane protein emerin by vesicular transport during ER stress. *eLife* **8**, e49796. doi: 10.7554/eLife.49796

Chen, C.-Y., Chi, Y.-H., Mutalif, R.A., Starost, M.F., Myers, T.G., Anderson, S.A., Stewart, C.L., Jeang, K.-T. (2012). Accumulation of the Inner Nuclear Envelope Protein Sun1 Is Pathogenic in Progeric and Dystrophic Laminopathies. *Cell* **149**, 565–577. doi: 10.1016/j.cell.2012.01.059

Chikashige, Y., Tsutsumi, C., Yamane, M., Okamasa, K., Haraguchi, T., Hiraoka, Y., 2006. Meiotic Proteins Bqt1 and Bqt2 Tether Telomeres to Form the Bouquet Arrangement of Chromosomes. Cell 125, 59–69. doi: /10.1016/j.cell.2006.01.048

Chikashige, Y., Yamane, M., Okamasa, K., Tsutsumi, C., Kojidani, T., Sato, M., Haraguchi, T., Hiraoka, Y. (2009). Membrane proteins Bqt3 and -4 anchor telomeres to the nuclear envelope to ensure chromosomal bouquet formation. *J. Cell Biol.* **187**, 413–427. doi: 10.1083/jcb.200902122

Christianson, J.C., Carvalho, P. (2022). Order through destruction: how ER-associated protein degradation contributes to organelle homeostasis. *EMBO J.* **41**, e109845 doi: 10.15252/embj.2021109845

Deng, M., Hochstrasser, M. (2006). Spatially regulated ubiquitin ligation by an ER/nuclear membrane ligase. *Nature* **443**, 827–831. doi: 10.1038/nature05170

633 Enam, C., Geffen, Y., Ravid, T., Gardner, R.G. (2018). Protein Quality Control Degradation
634 in the Nucleus. *Annu. Rev. Biochem.* **87**, 725–749. doi: 10.1146/annurev-biochem-
635 062917-012730

636 Foresti, O., Rodriguez-Vaello, V., Funaya, C., Carvalho, P. (2014). Quality control of inner
637 nuclear membrane proteins by the Asi complex. *Science* **346**, 751–755. doi:
638 10.1126/science.1255638

639 Franić, D., Zubčić, K., Boban, M. (2021). Nuclear Ubiquitin-Proteasome Pathways in
640 Proteostasis Maintenance. *Biomolecules* **11**, 54. doi: 10.3390/biom11010054

641 Gonzalez, Y., Saito, A., Sazer, S. (2012). Fission yeast Lem2 and Man1 perform fundamental
642 functions of the animal cell nuclear lamina. *Nucleus* **3**, 60–76. doi: 10.4161/nucl.18824

643 Gordon, C., McGurk, G., Dillon, P., Rosen, C., Hastie, N.D. (1993). Defective mitosis due to
644 a mutation in the gene for a fission yeast 265 protease subunit. *Nature* **366**, 355-357. doi:
645 10.1038/366355a0

646 Gordon, C., McGurk, G., Wallace, M., Hastie, N.D., 1996. A Conditional Lethal Mutant in
647 the Fission Yeast 26 S Protease Subunit *mts3*$^{+}$ Is Defective in Metaphase to Anaphase
648 Transition. *J. Biol. Chem.* **271**, 5704–5711. doi: 10.1074/jbc.271.10.5704

649 Habeck, G., Ebner, F.A., Shimada-Kreft, H., Kreft, S.G. (2015). The yeast ERAD-C
650 ubiquitin ligase Doa10 recognizes an intramembrane degron. *J. Cell Biol.* **209**, 261–273.
651 doi: 10.1083/jcb.201408088

652 Hirano, Y., Asakawa, H., Sakuno, T., Haraguchi, T., Hiraoka, Y. (2020a). Nuclear Envelope
653 Proteins Modulating the Heterochromatin Formation and Functions in Fission Yeast.
654 *Cells* **9**, 1908. doi: 10.3390/cells9081908

655 Hirano, Y., Y. Kinugasa, H. Osakada, T. Shindo, Y. Kubota, S. Shibata, T. Haraguchi, and Y.
656 Hiraoka. (2020b). Lem2 and Lnp1 maintain the membrane boundary between the nuclear
657 envelope and endoplasmic reticulum. *Commun. Biol*. **3**, 276. doi: 10.1038/s42003-020-
658 0999-9

659 Hirano, Y., Kinugasa, Y., Asakawa, H., Chikashige, Y., Obuse, C., Haraguchi, T., Hiraoka,
660 Y. (2018). Lem2 is retained at the nuclear envelope through its interaction with Bqt4 in
661 fission yeast. *Genes Cells* **23**, 122–135. doi: 10.1111/gtc.12557

662 Hirano, Y., Kinugasa, Y., Kubota, Y., Obuse, C., Haraguchi, T., Hiraoka, Y. (2023a) Inner
663 nuclear membrane proteins Lem2 and Bqt4 interact with different lipid synthesis
664 enzymes in fission yeast. *J. Biochem*. **174**, 33-46. doi: 10.1093/jb/mvad017

665 Hirano, Y., Ohno, Y., Kubota, Y., Fukagawa, T., Kihara, A., Haraguchi, T., Hiraoka, Y.
666 (2023b). Ceramide synthase homolog Tlc4 maintains nuclear envelope integrity via its
667 Golgi translocation. *J. Cell Sci* jcs260923. doi: 10.1242/jcs.260923

668 Hiraoka, Y., Maekawa, H., Asakawa, H., Chikashige, Y., Kojidani, T., Osakada, H.,
669 Matsuda, A., Haraguchi, T. (2011). Inner nuclear membrane protein Ima1 is dispensable
670 for intranuclear positioning of centromeres: *S. pombe* inner nuclear membrane proteins.
671 *Genes Cells* **16**, 1000–1011. doi: 10.1111/j.1365-2443.2011.01544.x

672 Huang, A., Tang, Y., Shi, X., Jia, M., Zhu, J., Yan, X., Chen, H., Gu, Y. (2020). Proximity
673 labeling proteomics reveals critical regulators for inner nuclear membrane protein
674 degradation in plants. *Nat. Commun.* **11**, 3284. doi: 10.1038/s41467-020-16744-1

675 Jarosch, E., Taxis, C., Volkwein, C., Bordallo, J., Finley, D., Wolf, D.H., Sommer, T. (2002).
676 Protein dislocation from the ER requires polyubiquitination and the AAA-ATPase
677 Cdc48. *Nat. Cell Biol.* **4**, 134–139. doi: 10.1038/ncb746

678 Khmelinskii, A., Blaszczak, E., Pantazopoulou, M., Fischer, B., Omnus, D.J., Le Dez, G.,
679 Brossard, A., Gunnarsson, A., Barry, J.D., Meurer, M., Kirrmaier, D., Boone, C., Huber,
680 W., Rabut, G., Ljungdahl, P.O., Knop, M. (2014). Protein quality control at the inner
681 nuclear membrane. *Nature* **516**, 410–413. doi: 10.1038/nature14096

682 Kinugasa, Y., Hirano, Y., Sawai, M., Ohno, Y., Shindo, T., Asakawa, H., Chikashige, Y.,
683 Shibata, S., Kihara, A., Haraguchi, T., Hiraoka, Y. (2019). The very-long-chain fatty
684 acid elongase Elo2 rescues lethal defects associated with loss of the nuclear barrier
685 function. *J. Cell Sci.* jcs.229021. doi: 10.1242/jcs.229021

686 Koch, B., Yu, H.-G. (2019). Regulation of inner nuclear membrane associated protein
687 degradation. *Nucleus* 10, 169–180. doi: /10.1080/19491034.2019.1644593

688 Koch, B.A., Jin, H., Tomko, R.J., Yu, H.-G., 2019. The anaphase-promoting complex
689 regulates the degradation of the inner nuclear membrane protein Mps3. *J. Cell Biol.* **218**,
690 839–854. doi: 10.1083/jcb.201808024

691 Kohda, T.A., Tanaka, K., Konomi, M., Sato, M., Osumi, M., Yamamoto, M. (2007). Fission
692 yeast autophagy induced by nitrogen starvation generates a nitrogen source that drives
693 adaptation processes. *Genes Cells* **12**, 155–170. doi: 10.1111/j.1365-2443.2007.01041.x

694 Krshnan, L., Siu, W.S., Van de Weijer, M., Hayward, D., Guerrero, E.N., Gruneberg, U.,
695 Carvalho, P. (2022). Regulated degradation of the inner nuclear membrane protein SUN2
696 maintains nuclear envelope architecture and function. *eLife* **11**, e81573. doi:
697 10.7554/eLife.81573.

698 Lord, S.J., K.B. Velle, R.D. Mullins, and L.K. Fritz-Laylin. (2020). SuperPlots:
699 Communicating reproducibility and variability in cell biology. *J. Cell Biol*. **219**,
700 e202001064. doi: 10.1083/jcb.202001064

701 Mannino, P.J., Lusk, C.P. (2022). Quality control mechanisms that protect nuclear envelope
702 identity and function. *J. Cell Biol.* **221**, e202205123. doi: 10.1083/jcb.202205123

703 Matsuyama, A., Arai, R., Yashiroda, Y., Shirai, A., Kamata, A., Sekido, S., Kobayashi, Y.,
704 Hashimoto, A., Hamamoto, M., Hiraoka, Y., Horinouchi, S., Yoshida, M., 2006.
705 ORFeome cloning and global analysis of protein localization in the fission yeast
706 Schizosaccharomyces pombe. *Nat. Biotechnol.* **24**, 841–847. doi: 10.1038/nbt1222

707 Mekhail, K., Moazed, D. (2010). The nuclear envelope in genome organization, expression
708 and stability. *Nat. Rev. Mol. Cell Biol.* **11**, 317–328. doi: 10.1038/nrm2894

709 Nakamura, Y., Arai, A., Takebe, Y., Masuda, M. (2011). A chemical compound for
710 controlled expression of nmt1-driven gene in the fission yeast *Schizosaccharomyces*
711 *pombe*. *Anal. Biochem.* **412**, 159–164. doi: 10.1016/j.ab.2011.01.039

712 Natarajan, N., Foresti, O., Wendrich, K., Stein, A., Carvalho, P. (2020). Quality Control of
713 Protein Complex Assembly by a Transmembrane Recognition Factor. *Mol. Cell* **77**, 108-
714 119. doi: 10.1016/j.molcel.2019.10.003

715 Nielsen, S., Poulsen, E., Rebula, C., Hartmann-Petersen, R., 2014. Protein Quality Control in
716 the Nucleus. *Biomolecules* **4**, 646–661. doi: 10.3390/biom4030646

717 Pantazopoulou, M., Boban, M., Foisner, R., Ljungdahl, P.O. (2016). Cdc48 and Ubx1
718 participate in an inner nuclear membrane associated degradation pathway that governs
719 the turnover of Asi1. *J. Cell Sci.* **129**, 3770-3780. doi: 10.1242/jcs.189332

720 Pawar, S., Kutay, U. (2021). The Diverse Cellular Functions of Inner Nuclear Membrane
721 Proteins. *Cold Spring Harb. Perspect. Biol.* **13**, a040477. doi:
722 10.1101/cshperspect.a040477

723 Pidoux, A. L., Armstrong, J. (1992) Analysis of the BiP gene and identification of an ER
724 retention signal in *Schizosaccharomyces pombe*. *EMBO J.* **11**, 1583-1591, doi:
725 10.1002/j.1460-2075.1992.tb05203.x

726 Rabinovich, E., Kerem, A., Fröhlich, K.-U., Diamant, N., Bar-Nun, S. (2002). AAA-ATPase
727 p97/Cdc48p, a Cytosolic Chaperone Required for Endoplasmic Reticulum-Associated
728 Protein Degradation. *Mol. Cell. Biol.* **22**, 626–634. doi: 10.1128/MCB.22.2.626-
729 634.2002

730 Ravid, T., Kreft, S.G., Hochstrasser, M. (2006). Membrane and soluble substrates of the
731 Doa10 ubiquitin ligase are degraded by distinct pathways. *EMBO J.* **25**, 533–543. doi:
732 10.1038/sj.emboj.7600946

733 Ruggiano, A., Foresti, O., Carvalho, P. (2014). ER-associated degradation: Protein quality
734 control and beyond. *J. Cell Biol.* **204**, 869–879. doi: 10.1083/jcb.201312042

735 Ruggiano, A., Mora, G., Carvalho, P. (2016). Spatial control of lipid droplet proteins by the
736 ERAD ubiquitin ligase Doa10. *EMBO J.* **35**,1644-1655. doi: 10.15252/embj.201593106

737 Santos-Rosa, H., Leung, J., Grimsey, N., Peak-Chew, S., Siniossoglou, S. (2005). The yeast
738 lipin Smp2 couples phospholipid biosynthesis to nuclear membrane growth. *EMBO J.*
739 **24**, 1931–1941. doi: 10.1038/sj.emboj.7600672

740 Sato, M., Dhut, S., Toda, T. (2005). New drug-resistant cassettes for gene disruption and
741 epitope tagging in *Schizosaccharomyces pombe*. *Yeast*. **22**, 583-591. doi:
742 10.1002/yea.1233

743 Schindelin, J., I. Arganda-Carreras, E. Frise, V. Kaynig, M. Longair, T. Pietzsch, S.
744 Preibisch, C. Rueden, S. Saalfeld, B. Schmid, J.-Y. Tinevez, D.J. White, V. Hartenstein,
745 K. Eliceiri, P. Tomancak, and A. Cardona. (2012). Fiji: an open-source platform for
746 biological-image analysis. *Nat. Methods.* **9**, 676-682. doi: 10.1038/nmeth.2019

747 Schuberth, C., Buchberger, A. (2005). Membrane-bound Ubx2 recruits Cdc48 to ubiquitin
748 ligases and their substrates to ensure efficient ER-associated protein degradation. *Nat.*
749 *Cell Biol.* **7**, 999-1006. doi: 10.1038/ncb1299.

750 Smoyer, C.J., Jaspersen, S.L. (2019). Patrolling the nucleus: inner nuclear membrane-
751 associated degradation. *Curr. Genet.* **65**, 1099–1106. doi: 10.1007/s00294-019-00971-1

752 Smoyer, C.J., Smith, S.E., Gardner, J.M., McCroskey, S., Unruh, J.R., Jaspersen, S.L. (2019).
753 Distribution of Proteins at the Inner Nuclear Membrane Is Regulated by the Asi1 E3
754 Ligase in *Saccharomyces cerevisiae*. *Genetics* **211**, 1269–1282. doi:
755 10.1534/genetics.119.301911

756 Steglich, B., Filion, G., van Steensel, B., Ekwall, K. (2012). The inner nuclear membrane
757 proteins Man1 and Ima1 link to two different types of chromatin at the nuclear periphery
758 in *S. pombe*. *Nucleus* **3**, 77–87. doi: 10.4161/nucl.18825

759 Swanson, R., Locher, M., Hochstrasser, M. (2001). A conserved ubiquitin ligase of the
760 nuclear envelope/endoplasmic reticulum that functions in both ER-associated and Matα2
761 repressor degradation. *Genes Dev.* **15**, 2660-2674. doi: 10.1101/gad.933301.

762 Takeda, K., Mori, A., Yanagida, M. (2011). Identification of Genes Affecting the Toxicity of
763 Anti-Cancer Drug Bortezomib by Genome-Wide Screening in S. pombe. *PLoS ONE* **6**,
764 e22021. doi: 10.1371/journal.pone.0022021

765 Takeda, K., Yanagida, M. (2005). Regulation of Nuclear Proteasome by Rhp6/Ubc2 through
766 Ubiquitination and Destruction of the Sensor and Anchor Cut8. *Cell* **122**, 393–405. doi:
767 10.1016/j.cell.2005.05.023

768 Tange, Y., Chikashige, Y., Takahata, S., Kawakami, K., Higashi, M., Mori, C., Kojidani, T.,
769 Hirano, Y., Asakawa, H., Murakami, Y., Haraguchi, T., Hiraoka, Y. (2016). Inner
770 nuclear membrane protein Lem2 augments heterochromatin formation in response to
771 nutritional conditions. *Genes Cells* **21**, 812–832. doi: 10.1111/gtc.12385

772 Tatebe, H., Yanagida, M. (2000). Cut8, essential for anaphase, controls localization of 26S
773 proteasome, facilitating destruction of cyclin and Cut2. *Curr. Biol.* **10**, 1329–1338. doi:
774 10.1016/S0960-9822(00)00773-9

775 Toyama, B.H., Savas, J.N., Park, S.K., Harris, M.S., Ingolia, N.T., Yates, J.R., Hetzer, M.W.
776 (2013). Identification of Long-Lived Proteins Reveals Exceptional Stability of Essential
777 Cellular Structures. *Cell* **154**, 971–982. doi: 10.1016/j.cell.2013.07.037

778 Tsai, P.-L., Zhao, C., Turner, E., Schlieker, C. (2016). The Lamin B receptor is essential for
779 cholesterol synthesis and perturbed by disease-causing mutations. *eLife* **5**, e16011. doi:
780 10.7554/eLife.16011

781 Vembar, S.S., Brodsky, J.L. (2008). One step at a time: endoplasmic reticulum-associated
782 degradation. *Nat. Rev. Mol. Cell Biol.* **9**, 944–957. doi: 10.1038/nrm2546

783 Wach, A. (1996). PCR-synthesis of marker cassettes with long flanking homology regions for
784 gene disruptions in *S. cerevisiae*. *Yeast*. **12**, 259-265. doi: 10.1002/(SICI)1097-
785 0061(19960315)12:3%3C259::AID-YEA901%3E3.0.CO;2-C

786 Wolf, D.H., Stolz, A. (2012). The Cdc48 machine in endoplasmic reticulum associated
787 protein degradation. *Biochim. Biophys. Acta.* **1823**, 117–124. doi:
788 10.1016/j.bbamcr.2011.09.002

789 Ye, Y., Meyer, H.H., Rapoport, T.A. (2001). The AAA ATPase Cdc48/p97 and its partners
790 transport proteins from the ER into the cytosol. *Nature* **414**, 652–656. doi:
791 10.1038/414652a

792

793 **Figure legends**

794 **Fig. 1. Bqt4 protein is degraded by the ubiquitin-proteasome system**

795 (A, B) Cells expressing GFP-Bqt4 in the *bqt3*$^{+}$ or *bqt3*Δ background were treated with
796 vehicle (+DMSO) or the proteasome inhibitor bortezomib (+BZ) for 4 h and subjected to
797 microscopic observation (A) or western blotting (B). (A) Fluorescence microscopy images of
798 GFP-Bqt4 (upper panels); bright-field images (lower panels). Bar, 10 μm. (B) Protein
799 amounts of GFP-Bqt4 and β-actin were detected by anti-GFP and anti-β-actin antibodies,
800 respectively. Molecular weight markers are shown on the left.

801 (C, D) Cells harboring *mts3-1* in the *bqt3*$^{+}$ or *bqt3*Δ background were cultured at a
802 nonpermissive temperature (36°C) for 4 h and subjected to microscopic observation (C) or
803 western blotting (D). (C) Fluorescence microscopy images of GFP-Bqt4 (upper panels);
804 bright-field images (lower panels). Bar, 10 μm. (D) Protein amounts of GFP-Bqt4 and β-actin
805 were detected as in (B). The asterisk in (D) indicates non-specific bands.

806 (E) Polyubiqutination of Bqt4 protein. Cells expressing GFP or GFP-Bqt4 in the *bqt3*$^{+}$ or
807 *bqt3*Δ background were treated with vehicle (+DMSO) or the proteasome inhibitor
808 bortezomib (+BZ) for 4 h. After denaturing the proteins, GFP and GFP-Bqt4 were
809 immunoprecipitated with anti-GFP antibody (IP). The precipitated proteins were detected by
810 anti-ubiquitin or anti-GFP antibodies, respectively (IB). β-actin was used as a loading
811 control. Molecular weight markers are shown on the left.

812 (F) Bqt4 degradation rate in *bqt3*$^{+}$ or *bqt3*Δ cells. The *bqt3*$^{+}$ or *bqt3*Δ cells expressing GFP or
813 GFP-Bqt4 were cultured in cycloheximide-containing YES medium for the time indicated on
814 the top of the panels. The level of GFP and GFP-Bqt4 in the cells were detected by western
815 blotting. β-actin was used as a loading control. Asterisk represents non-specific band.
816 Molecular weight markers are shown on the left.

817 (G) No Bqt4 degradation by the lysosome-autophagy system. Deletion of *atg1* (*atg1*Δ) or
818 *isp6* (*isp6*Δ) was introduced into the *bqt3*Δ cells. Protein amounts of GFP-Bqt4 and β-actin in
819 these cells were detected as in (B).Molecular weight markers are shown on the left.
820
821 **Fig. 2. Bqt4 degradation occurs in the nucleus**
822 Cells harboring *cut8-563 ts* mutation in the *bqt3*$^{+}$ or *bqt3*Δ background were cultured at a
823 nonpermissive temperature (36°C) for 4 h and subjected to microscopic observation (A) or
824 western blotting (B). (A) Fluorescence images of GFP-Bqt4 (upper panels) and bright-field
825 images (lower panels). Bar, 10 μm. (B) Protein levels of GFP-Bqt4 and β-actin were detected
826 using anti-GFP and anti-β-actin antibodies, respectively. Asterisks indicate non-specific
827 bands. The molecular weight markers are shown on the left.
828
829 **Fig. 3. Bqt4 is a substrate of the Doa10 complex**
830 (A, B) Cells harboring *hrd1* (*hrd1*Δ), *doa10* (*doa10*Δ) single deletion, or *hrd1* and *doa10*
831 double deletion (*hrd1*Δ *doa10*Δ) in *bqt3*Δ background were cultured at 30°C for 16 h, and
832 then subjected to microscopic observation (A) or western blotting (B). (A) Fluorescence
833 images of GFP-Bqt4 (upper panels) and bright-field images (lower panels). Bar, 10 μm. (B)
834 Protein levels of GFP-Bqt4 and β-actin were detected using anti-GFP and anti-β-actin
835 antibodies, respectively.
836 (C, D) Cells harboring *ubc6* (*ubc6*Δ), *ubc7* (*ubc7*Δ) single deletion, or *ubc6* and *ubc7* double
837 deletion (*ubc6*Δ *ubc7*Δ) in *bqt3*Δ background were cultured at 30°C for 16 h, and then
838 subjected to microscopic observation (C) or western blotting (D). (C) Fluorescence images of
839 GFP-Bqt4 (upper panels) and bright-field images (lower panels). Bar, 10 μm. (D) Protein
840 levels of GFP-Bqt4 and β-actin were detected using anti-GFP and anti-β-actin antibodies,

841 respectively. Asterisks indicate non-specific bands. The molecular weight markers are shown
842 on the left.
843
844 **Fig. 4. Bqt4 is an integral membrane protein**
845 (A) Cells expressing GFP-Bqt4, Ish1-GFP, or GFP-ADEL were mixed and lysed by bead
846 beating. After isolating membrane fraction, the membrane was treated under various
847 conditions as shown on the top. The extracts were fractionated by ultracentrifugation into
848 supernatant (S) and pellet (P), and then GFP-tagged proteins in each fraction were detected
849 by western blotting. Molecular weight markers are shown on the left. Values at the middle
850 panel represent the GFP-Bqt4 intensity ratio in supernatant and pellet fractions.
851 (B) The *bqt3*Δ *doa10*Δ cells expressing GFP-Bqt4 were treated as described in A and then
852 GFP-tagged proteins in each fraction were detected by western blotting. Molecular weight
853 markers are shown on the left. Values at the middle panel represent the GFP-Bqt4 intensity
854 ratio in supernatant and pellet fractions.
855
856 **Fig. 5. Removal of Bqt4 requires the Cdc48 retrotranslocation complex**
857 (A) The Cdc48 mutant used in this study. Left panel: the amino acid sequence alignment
858 around the D1 and D2 domains of *S. pombe* (*Sp*) and *S. cerevisiae* (*Sc*) Cdc48. Gray and light
859 gray shades denote identical and similar amino acids, respectively (top and bottom). The
860 amino acids indicated by red (P267 and A550; correspond to red stars in the schematic
861 diagram in the middle) are both mutated in this study (P267L/A550T). Right panel: the
862 mutation sites are shown in the predicted three-dimensional structure of Cdc48 by
863 AlphaFold2 (https://alphafold.ebi.ac.uk/entry/Q9P3A7).

864 (B) Temperature sensitivity of *cdc48-P267L/A550T* mutant. Five-fold serially diluted cells
865 harboring *cdc48-P267L/A550T* mutant were spotted on the YES plate, and cultured at
866 different temperatures as indicated at the top.
867 (C, D) Effect of hypomorphic mutation of *cdc48* on Bqt4 degradation. Cells harboring the
868 *cdc48-P267L/A550T* mutant in the *bqt3*$^{+}$ or *bqt3*Δ background were cultured at a
869 nonpermissive temperature (16°C) for 15 h and subjected to microscopic observation (C) or
870 western blotting (D). (C) Left panels: Fluorescence images of GFP-Bqt4 (upper panels);
871 bright-field images (lower panels). Bar: 10 μm. Right panel: the fluorescence intensities in
872 the nuclei were quantified and the relative values were plotted. The mean values are plotted
873 with standard deviation on the right panel. The number of the cells analyzed is shown at the
874 bottom. ****$p < 0.0001$ via two-tailed unpaired student's *t*-test. (D) Protein amounts of GFP-
875 Bqt4 and β-actin were detected by anti-GFP and anti-β-actin antibodies, respectively.
876 Molecular weight markers are shown on the left.
877
878 **Fig. 6. The C-terminal sequence of Bqt4 is a degron**
879 (A) The C-terminal fragments of Bqt4 are shown as a cartoon on the left. These fragments
880 were expressed as GFP-fused proteins in the *bqt3*$^{+}$ or *bqt3*Δ cells. The cells were treated with
881 vehicle (+DMSO) or the proteasome inhibitor bortezomib (+BZ) for 4 h and then observed
882 by fluorescence microscopy. Bars: 10 μm.
883 (B) Interaction between C-terminal truncated fragments of Bqt4 and full-length Bqt3 was
884 examined by the yeast two-hybrid assay. AD, the transcriptional activation domain only (vec)
885 or fused to GFP-Bqt4 fragments were expressed from the pGADT7 plasmid. BD, the DNA-
886 binding domain only (vec) or fused to full-length Bqt3 were expressed from the pGBKT7
887 plasmid. The combination of AD- and BD-fused fragments are summarized at the right. The
888 cells harboring both plasmids were cultured on control and selective medium.

889 (C) Membrane association assay of GFP-Bqt4C$^{369-425}$. The fragments were extracted from the
890 membrane as described in Fig. 4A and detected by western blotting. S and P represent
891 supernatant and pellet, respectively. Molecular weight markers are shown on the left. Values
892 at the bottom represent the GFP-Bqt4 intensity ratio in supernatant and pellet fractions.
893 (D) Schematic diagram of roles of the C-terminus of Bqt4.
894
895 **Fig. 7. Excess Bqt4 causes nuclear envelope deformation**
896 (A) Left panels: Fluorescence images of Ish1-GFP in *bqt4*$^{+}$ or *bqt4*Δ cells. Ish1-GFP was
897 used as a nuclear membrane marker (Asakawa et al., 2022). The cells were treated with
898 vehicle (+DMSO) or the proteasome inhibitor bortezomib (+BZ) for 4 h. The images were
899 deconvoluted using built-in SoftWoRx software with default settings. Bar: 10 μm. Right
900 panel: The roundness index of the nuclei in these cells was measured from three independent
901 experiments (blue, green, and red) and plotted as a superplot (Lord et al., 2020) (right panel).
902 The roundness index of 1 indicates a perfect circle. The solid blue circle, green triangle, and
903 red square represent the mean values in each experiment. Black horizontal lines represent the
904 mean values for all data shown with standard deviations. *n* at the bottom right represents the
905 total number of cells analyzed. ****$p < 0.0001$ via two-tailed unpaired student's *t*-test.
906 (B-D) NE deformation due to Bqt4 overexpression. (B) Representative fluorescence images
907 of GFP-Bqt4 in *bqt3*$^{+}$ cells. GFP-Bqt4 was overexpressed under the control of the *nmt1*
908 promoter in the presence or absence of YAM2 in the EMMG for 20 h. The YAM2
909 concentrations are shown in the images. To improve visibility, the contrast of the image was
910 adjusted to the intensity range indicated at the bottom. Bar: 10 μm. (C) GFP-Bqt4 protein
911 levels. Protein levels of GFP-Bqt4 shown in (B) were determined by western blotting. β-actin
912 was used for loading control. Because the full expression of GFP-Bqt4 (0 μM YAM2) was
913 strong, 1/10 (0.5 μg), 1/5 (1 μg), and 1 (5 μg) relative amounts of total proteins were

914 electrophoresed. Short- and long-exposure images are shown in upper and lower panels,
915 respectively. The bands indicated by asterisks in the bottom panel are saturated. The
916 molecular weight markers are shown on the left. (D) Roundness index of the nuclei was
917 mesured in BZ-treated (*bqt4*p, BZ; blue) and YAM2-treated (*nmt1*p+YAM2; green) *bqt3*$^{+}$
918 cells overexpressing Bqt4. The roundness index was also measured in WT (*bqt4*p, -; red).
919 The values were plotted with mean ± SD. *n* on the horizontal axis represents the number of
920 cells analyzed. Significance was assessed using the Tukey's test. * $P < 0.05$; **** $P <$
921 0.0001; ns, not significant.
922 (E) Growth defects by Bqt4 overproduction. GFP-Bqt4 was overexpressed in *bqt4* (*bqt4p*) or
923 *nmt1* promoter (*nmt1p*) in *bqt3*$^{+}$ or *bqt3*Δ cells. Five-fold serially diluted cells were spotted
924 onto EMMG plates in the presence or absence of thiamine for four days. WT indicates
925 wildtype.
926
927 **Fig. 8. A model of INM protein degradation of Bqt4**
928 Excess Bqt4, with the exposed TMD as a degradation signal, is recognized and ubiquitinated
929 by INM-associated E3 ubiquitin ligase complexes, including Doa10 and additional
930 unidentified E3 ligases. Ubiquitinated Bqt4 is then transferred to the nuclear proteasome for
931 proteolysis. Degradation of Bqt4 requires the AAA-ATPase Cdc48 complex.

Figure 1

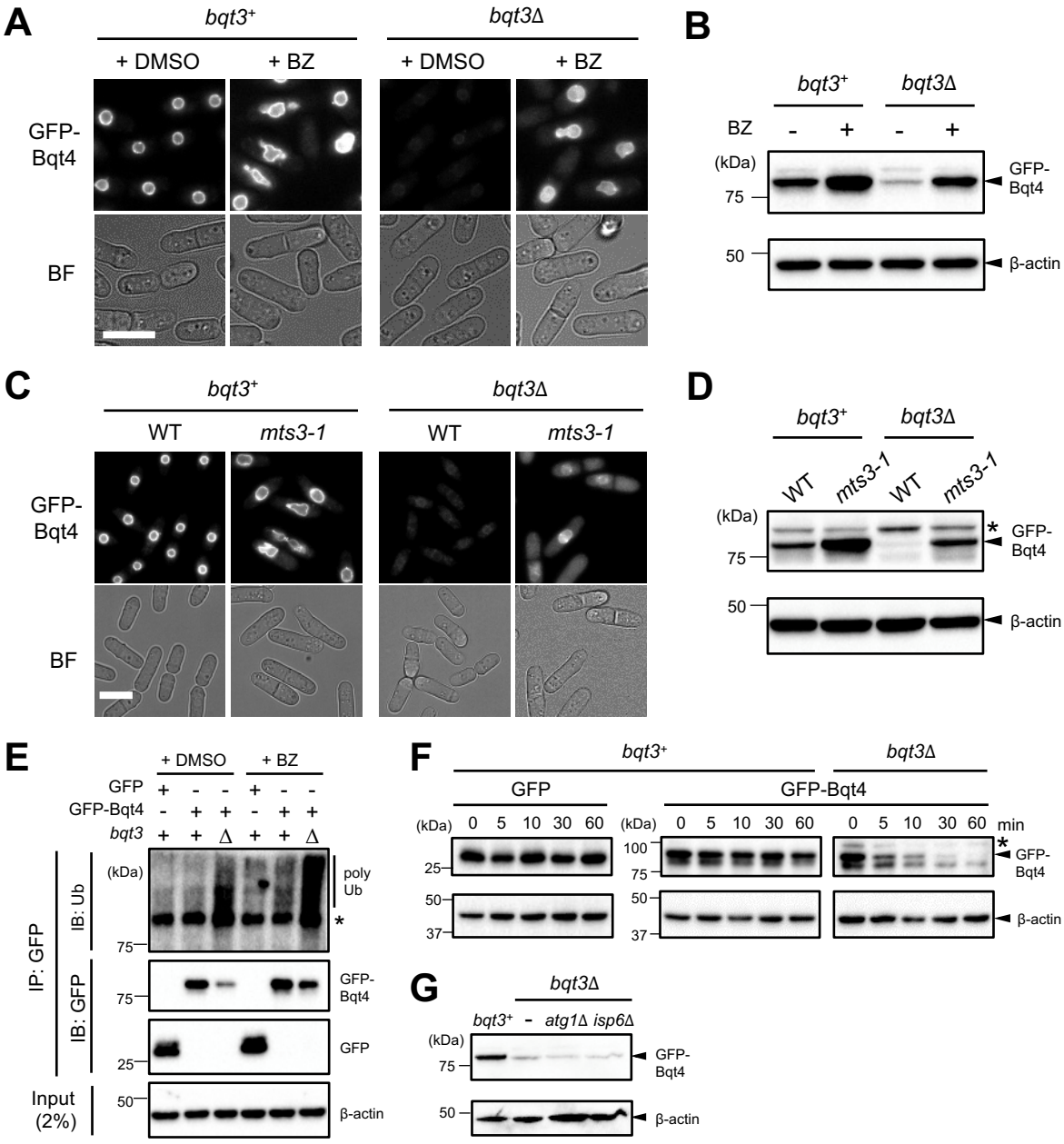
A
bqt3+
bqt3Δ
+ DMSO
+ BZ
+ DMSO
+ BZ
GFP-Bqt4
BF
B
bqt3+
bqt3Δ
BZ
-
+
-
+
(kDa)
75
50
GFP-Bqt4
β-actin
C
bqt3+
bqt3Δ
WT
mts3-1
WT
mts3-1
GFP-Bqt4
BF
D
bqt3+
bqt3Δ
WT
mts3-1
WT
mts3-1
(kDa)
75
50
*
GFP-Bqt4
β-actin
E
+ DMSO
+ BZ
GFP
GFP-Bqt4
bqt3
Δ
Δ
IP: GFP
IB: Ub
IB: GFP
(kDa)
poly Ub
*
75
25
GFP-Bqt4
GFP
Input (2%)
50
β-actin
F
bqt3+
bqt3Δ
GFP
GFP-Bqt4
(kDa)
0 5 10 30 60
min
25
50
37
100
75
*
GFP-Bqt4
β-actin
G
bqt3Δ
bqt3+
-
atg1Δ
isp6Δ
(kDa)
75
50
GFP-Bqt4
β-actin

Figure 2

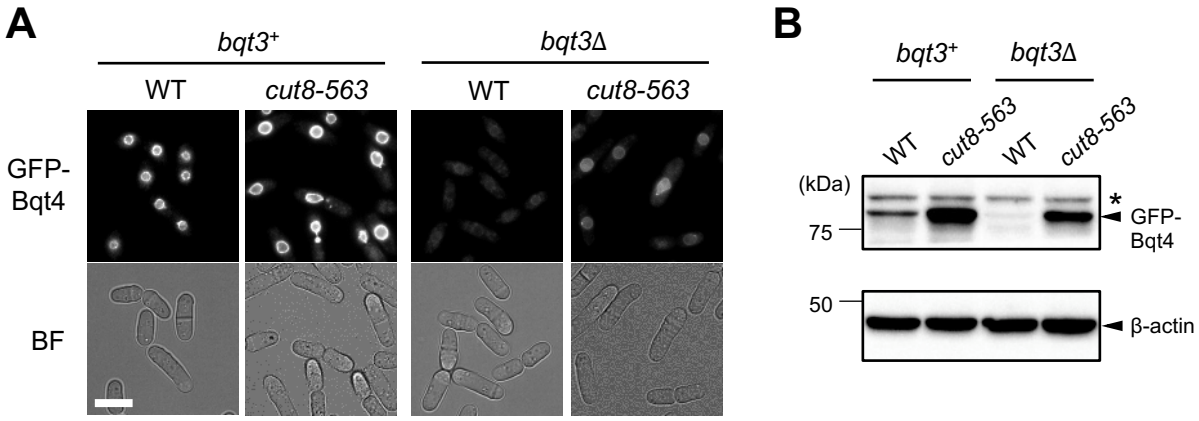
A
bqt3+
bqt3Δ
WT
cut8-563
WT
cut8-563
GFP-Bqt4
BF
B
bqt3+
bqt3Δ
WT
cut8-563
WT
cut8-563
(kDa)
75
50
*
GFP-Bqt4
β-actin

Figure 3

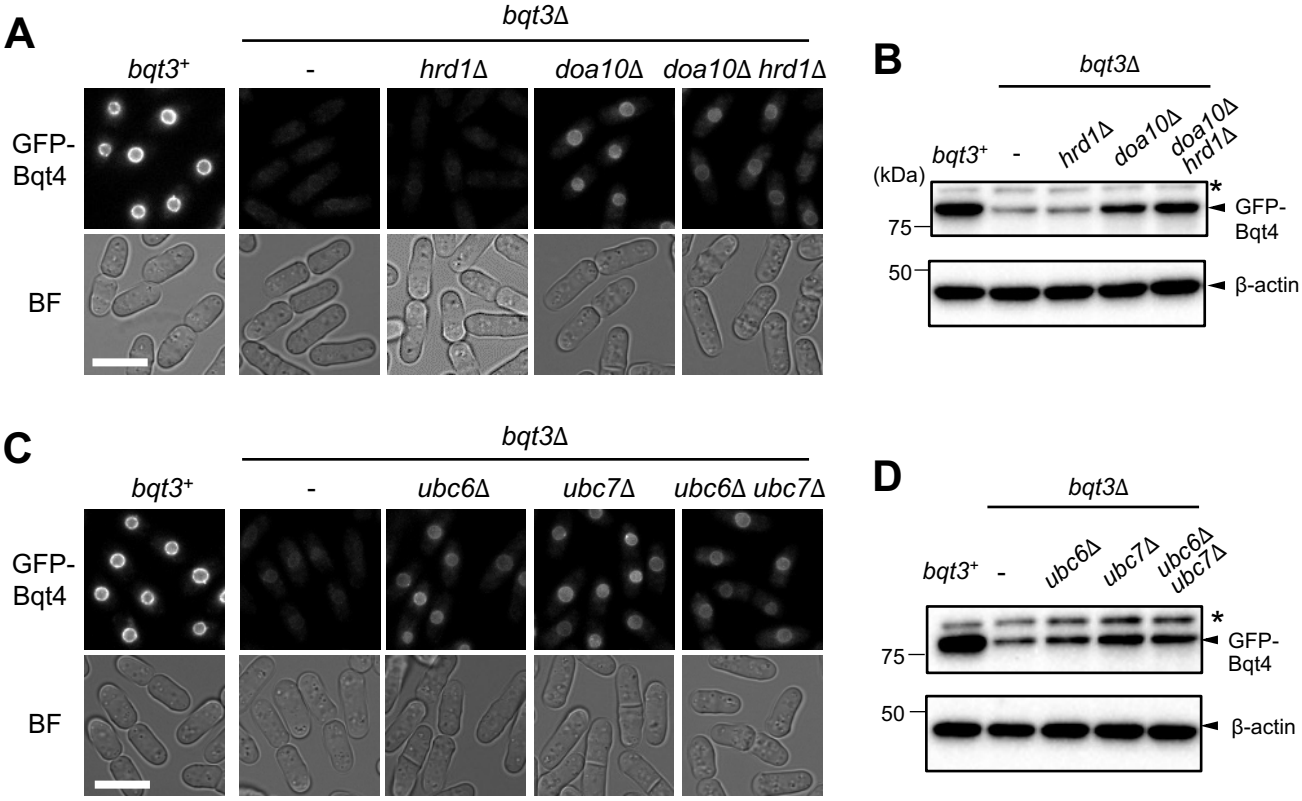
A
bqt3Δ
bqt3+
-
hrd1Δ
doa10Δ
doa10Δ hrd1Δ
GFP-Bqt4
BF
B
bqt3Δ
bqt3+
-
hrd1Δ
doa10Δ
doa10Δ hrd1Δ
(kDa)
75
50
*
GFP-Bqt4
β-actin
C
bqt3Δ
bqt3+
-
ubc6Δ
ubc7Δ
ubc6Δ ubc7Δ
GFP-Bqt4
BF
D
bqt3Δ
bqt3+
-
ubc6Δ
ubc7Δ
ubc6Δ ubc7Δ
75
50
*
GFP-Bqt4
β-actin

Figure 4

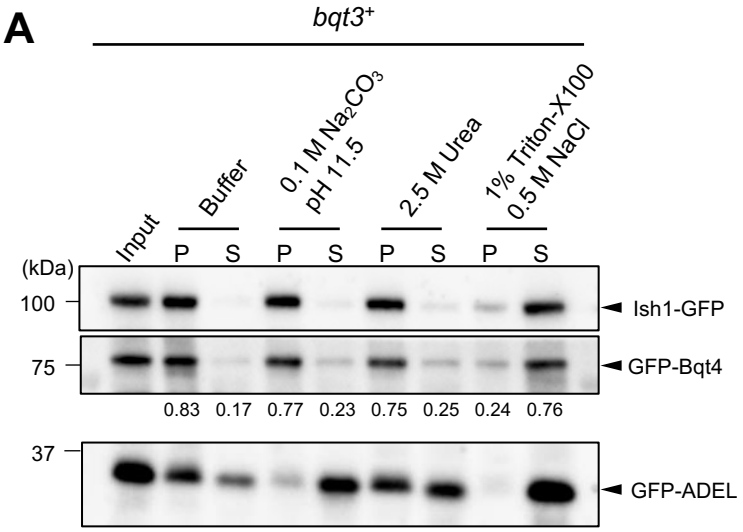
A
bqt3+
Input
Buffer
0.1 M Na2CO3 pH 11.5
2.5 M Urea
1% Triton-X100 0.5 M NaCl
P S P S P S P S
(kDa)
100
75
37
Ish1-GFP
GFP-Bqt4
GFP-ADEL
0.83 0.17 0.77 0.23 0.75 0.25 0.24 0.76

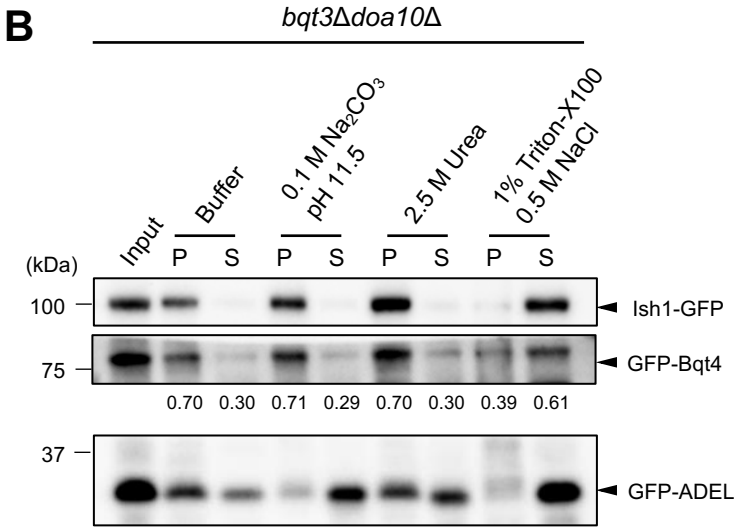
B
bqt3Δdoa10Δ
Input
Buffer
0.1 M Na2CO3 pH 11.5
2.5 M Urea
1% Triton-X100 0.5 M NaCl
P S P S P S P S
(kDa)
100
75
37
Ish1-GFP
GFP-Bqt4
GFP-ADEL
0.70 0.30 0.71 0.29 0.70 0.30 0.39 0.61

Figure 5

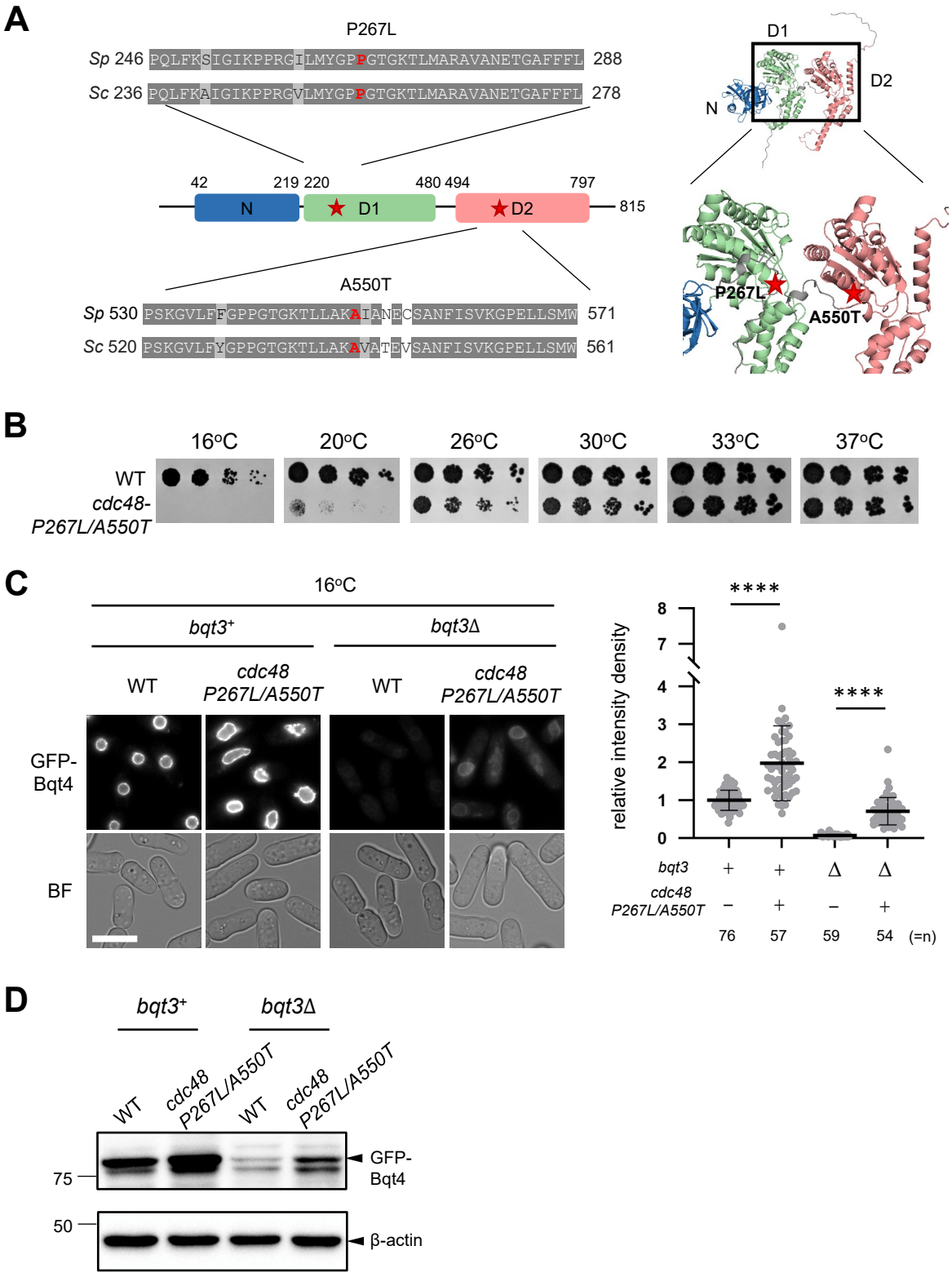
A
P267L
Sp 246 PQLFKSIGIKPPRGILMYGPPGTGKTLMARAVANETGAFFFL 288
Sc 236 PQLFKAIGIKPPRGVLMYGPPGTGKTLMARAVANETGAFFFL 278
42
219 220
480 494
797
N
D1
D2
815
A550T
Sp 530 PSKGVLFFGPPGTGKTLLAKAIANECSANFISVKGPELLSMW 571
Sc 520 PSKGVLFYGPPGTGKTLLAKAVATEVSANFISVKGPELLSMW 561
D1
D2
N
P267L
A550T
B
16°C
20°C
26°C
30°C
33°C
37°C
WT
cdc48-
P267L/A550T
C
16°C
bqt3+
bqt3Δ
WT
cdc48
P267L/A550T
WT
cdc48
P267L/A550T
GFP-
Bqt4
BF
relative intensity density
****
****
bqt3
cdc48
P267L/A550T
76
57
59
54
(=n)
D
bqt3+
bqt3Δ
WT
cdc48
P267L/A550T
WT
cdc48
P267L/A550T
75
50
GFP-
Bqt4
β-actin

Figure 6

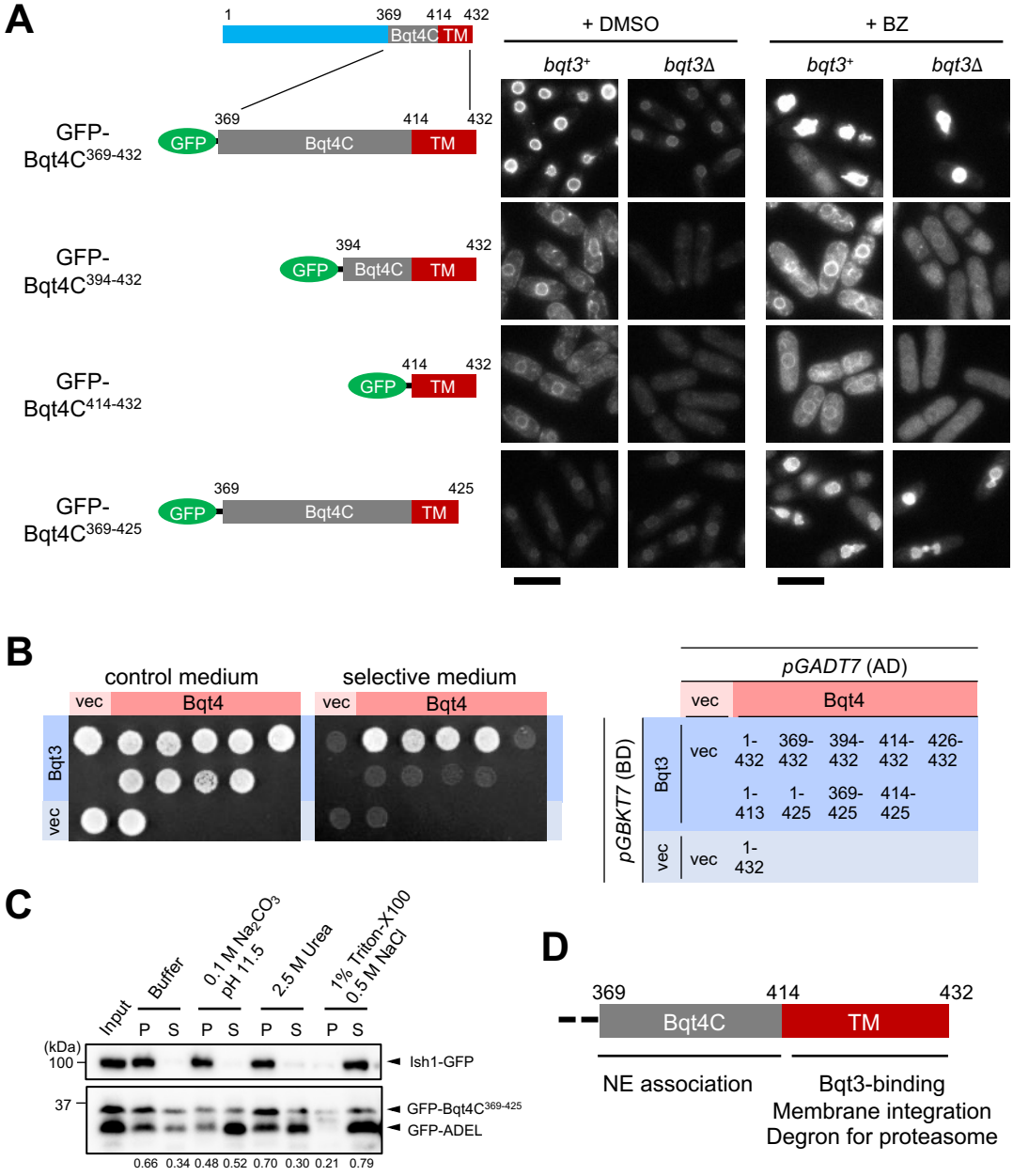
A
1
369
414
432
Bqt4C
TM
+ DMSO
+ BZ
bqt3+
bqt3Δ
GFP-Bqt4C369-432
GFP-Bqt4C394-432
GFP-Bqt4C414-432
GFP-Bqt4C369-425
GFP
394
425
B
control medium
selective medium
vec
Bqt4
Bqt3
pGADT7 (AD)
pGBKT7 (BD)
1-432
369-432
394-432
414-432
426-432
1-413
1-425
369-425
414-425
C
Input
Buffer
0.1 M Na2CO3 pH 11.5
2.5 M Urea
1% Triton-X100 0.5 M NaCl
P S P S P S P S
(kDa)
100
37
Ish1-GFP
GFP-Bqt4C369-425
GFP-ADEL
0.66 0.34 0.48 0.52 0.70 0.30 0.21 0.79
D
NE association
Bqt3-binding
Membrane integration
Degron for proteasome

Figure 7

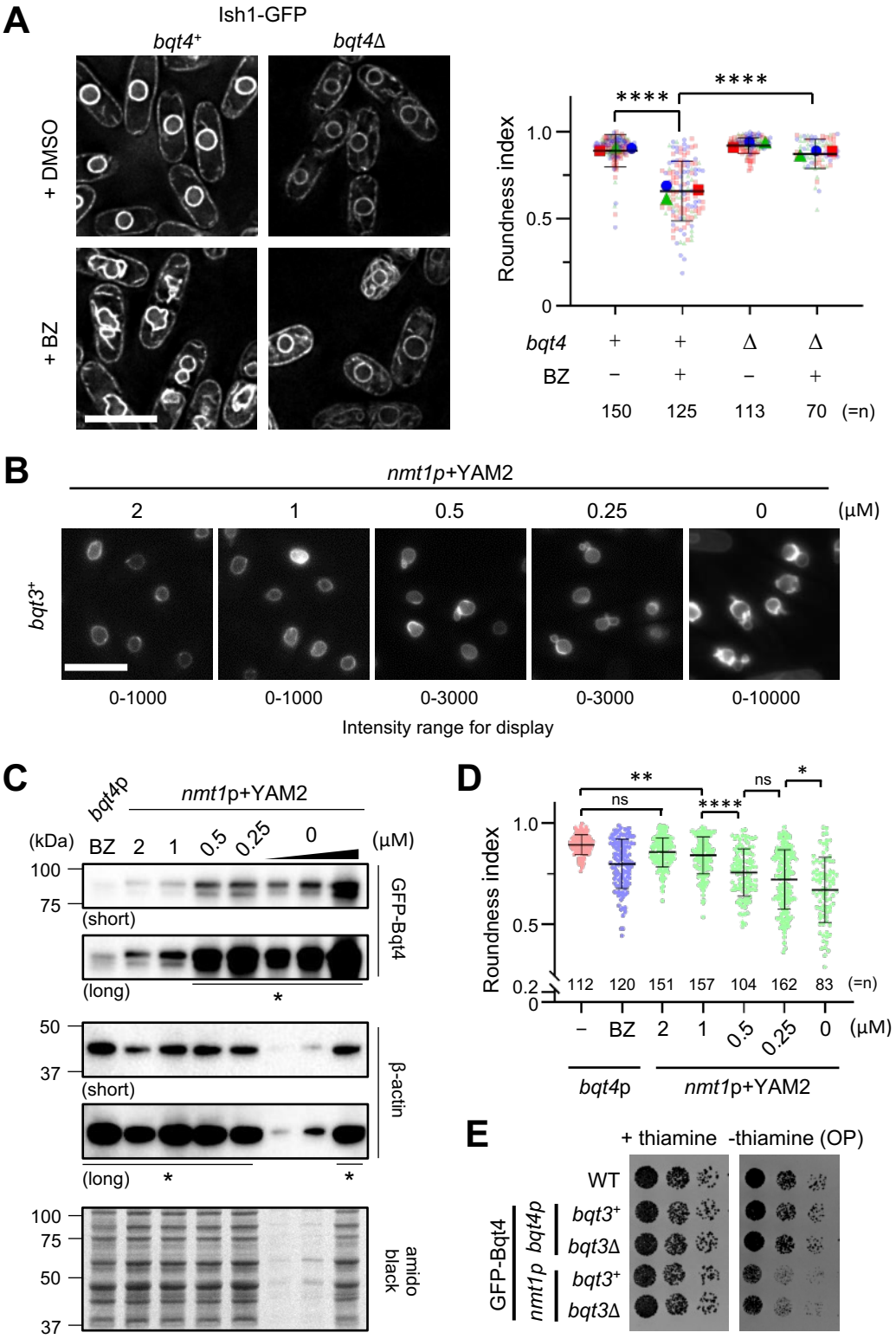
A
Ish1-GFP
bqt4+
bqt4Δ
+ DMSO
+ BZ
Roundness index
1.0
0.5
0
****
****
bqt4
+
+
Δ
Δ
BZ
−
+
−
+
150
125
113
70
(=n)
B
nmt1p+YAM2
2
1
0.5
0.25
0
(μM)
bqt3+
0-1000
0-1000
0-3000
0-3000
0-10000
Intensity range for display
C
bqt4p
nmt1p+YAM2
(kDa)
BZ
2
1
0.5
0.25
0
(μM)
100
75
(short)
(long)
GFP-Bqt4
50
37
β-actin
amido black
D
Roundness index
1.0
0.5
0.2
0
**
ns
****
ns
*
112
120
151
157
104
162
83
(=n)
−
BZ
2
1
0.5
0.25
0
(μM)
bqt4p
nmt1p+YAM2
E
+ thiamine
-thiamine (OP)
WT
GFP-Bqt4
bqt4p
bqt3+
bqt3Δ
nmt1p
bqt3+
bqt3Δ

Figure 8

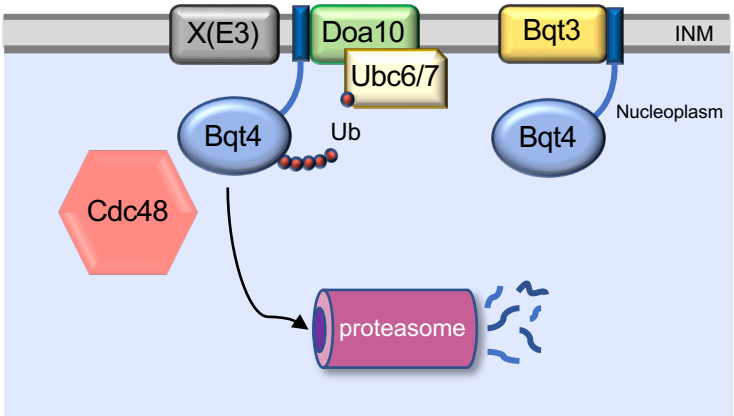
X(E3)
Doa10
Bqt3
INM
Ubc6/7
Bqt4
Ub
Bqt4
Nucleoplasm
Cdc48
proteasome

Supplementary Table 1. Yeast strains used in this study

S. pombe strains

Strain	Genotype	Source	Figure
TL204	*h⁻ bqt4Δ::hph lys1⁺::bqt4p-GFP-bqt4*	This study	1A-G, 2A, B, 3A-D, 4A, 5C, D 7C-E, S1, S3A, B, S5
TL205	*h⁻ bqt4Δ::hph lys1⁺::bqt4p-GFP-bqt4 bqt3Δ::NAT*	This study	1A-G, 2A, B, 3A-D, 5C, D, 7E, S1, S2, S3A, B, S5
TL288	*h⁻ bqt4Δ::hph lys1⁺::bqt4p-GFP-bqt4 mts3-1*	This study	1C, D
TL289	*h⁻ bqt4Δ::hph bqt3Δ::NAT lys1⁺::bqt4p-GFP-bqt4 mts3-1*	This study	1C, D
H1N95	*h⁻ bqt4Δ::hph lys1⁺::bqt4p-GFP*	This study	1E
H1N2114	*h⁻ bqt4Δ::kan^r bqt3Δ::NAT aur1^r::mCherry-bqt3 lys1⁺::bqt4p-GFP*	This study	1F
TL233	*h⁻ bqt4Δ::hph bqt3Δ::NAT lys1⁺::bqt4p-GFP-bqt4 isp6Δ::bsd*	This study	1G
TL234	*h⁻ bqt4Δ::hph bqt3Δ::NAT lys1⁺::bqt4p-GFP-bqt4 atg1Δ:: kan^r*	This study	1G
TL290	*h⁻ bqt4Δ::hph lys1⁺::bqt4p-GFP-bqt4 cut8-563*	This study	2A, B
TL291	*h⁻ bqt4Δ::hph bqt3Δ::NAT lys1⁺::bqt4p-GFP-bqt4 cut8-563*	This study	2A, B
TL215	*h⁻ bqt4Δ::hph bqt3Δ::NAT lys1⁺::bqt4p-GFP-bqt4 doa10Δ::bsd*	This study	3A, B, 4B, S2, S3A, B
TL219	*h⁻ bqt4Δ::hph bqt3Δ::NAT lys1⁺::bqt4p-GFP-bqt4 hrd1Δ:: kan^r*	This study	3A, B, S2
TL236	*h⁻ bqt4Δ::hph bqt3Δ::NAT lys1⁺::bqt4p-GFP-bqt4 doa10Δ::bsd hrd1Δ:: kan^r*	This study	3A, B
TL220	*h⁻ bqt4Δ::hph bqt3Δ::NAT lys1⁺::bqt4p-GFP-bqt4 ubc7Δ:: kan^r*	This study	3C, D
TL221	*h⁻ bqt4Δ::hph bqt3Δ::NAT lys1⁺::bqt4p-GFP-bqt4 ubc6Δ:: kan^r*	This study	3C, D
TL266	*h⁻ bqt4Δ::hph bqt3Δ::NAT lys1⁺::bqt4p-GFP-bqt4 ubc6Δ:: kan^r ubc7Δ::bsd*	This study	3C, D
HA1382-3D	*h⁻ lys1-131 ura4-D18 leu1-32 bqt3Δ::LEU2 aur1^r::bqt3p-GFP-bqt3*	This study	4A
H1N429	*h⁻ lys1⁺::ish1-GFP*	This study	4A, B, 6C, 7A
H1N789	*h⁻ lys1+::nmt41p-SS-GFP-ADEL*	This study	4A, B, 6C
h-972	*h⁻*	Laboratory stock	5B, 7E
TL311	*h⁻ lys1-131 cdc48Δ:: kan^r aur1^r::cdc48p-cdc48-P267L/A550T*	This study	5B
TL306	*h⁻ bqt4Δ::hph lys1⁺::bqt4p-GFP-bqt4 cdc48Δ:: kan^r aur1^r::cdc48p-cdc48-P267L/A550T*	This study	5C, D, S5
TL307	*h⁻ bqt4Δ::hph lys1⁺::bqt4p-GFP-bqt4 bqt3Δ::NAT cdc48Δ:: kan^r aur1^r::cdc48p-cdc48-P267L/A550T*	This study	5C, D, S5
TL242	*h⁻ bqt4Δ::hph lys1⁺::bqt4p-GFP-bqt4C$^{369-432}$*	This study	6A
TL243	*h⁻ bqt4Δ::hph bqt3Δ::NAT lys1⁺::bqt4p-GFP-bqt4C$^{369-432}$*	This study	6A
TL246	*h⁻ bqt4Δ::hph lys1⁺::bqt4p-GFP-bqt4C$^{394-432}$*	This study	6A
TL247	*h⁻ bqt4Δ::hph bqt3Δ::NAT lys1⁺::bqt4p-GFP-bqt4C$^{394-432}$*	This study	6A
TL248	*h⁻ bqt4Δ::hph lys1⁺::bqt4p-GFP-bqt4C$^{414-432}$*	This study	6A
TL249	*h⁻ bqt4Δ::hph bqt3Δ::NAT lys1⁺::bqt4p-GFP-bqt4C$^{414-432}$*	This study	6A
TL250	*h⁻ bqt4Δ::hph lys1⁺::bqt4p-GFP-bqt4C$^{369-425}$*	This study	6A, C, S7
TL251	*h⁻ bqt4Δ::hph bqt3Δ::NAT lys1⁺::bqt4p-GFP-bqt4C$^{369-425}$*	This study	6A
H1N546	*h⁺ bqt4Δ::hph lys1⁺::ish1-GFP*	This study	7A
TL206	*h⁻ bqt4Δ::hph lys1⁺::nmt1p-GFP-bqt4*	This study	7B-E
TL207	*h⁻ bqt4Δ::hph lys1⁺::nmt1p-GFP-bqt4 bqt3Δ::NAT*	This study	7E
TL286	*h⁻ bqt4Δ::hph lys1⁺::bqt4p-GFP-bqt4 mts2-1*	This study	S1
TL287	*h⁻ bqt4Δ::hph bqt3Δ::NAT lys1⁺::bqt4p-GFP-bqt4 mts2-1*	This study	S1
TL222	*h⁻ bqt4Δ::hph bqt3Δ::NAT lys1⁺::bqt4p-GFP-bqt4 meu34Δ:: kan^r*	This study	S2
TL224	*h⁻ bqt4Δ::hph bqt3Δ::NAT lys1⁺::bqt4p-GFP-bqt4 san1Δ:: kan^r*	This study	S2
TL225	*h⁻ bqt4Δ::hph bqt3Δ::NAT lys1⁺::bqt4p-GFP-bqt4 ubr1Δ:: kan^r*	This study	S2
TL226	*h⁻ bqt4Δ::hph bqt3Δ::NAT lys1⁺::bqt4p-GFP-bqt4 ubr11Δ:: kan^r*	This study	S2
TL227	*h⁻ bqt4Δ::hph bqt3Δ::NAT lys1⁺::bqt4p-GFP-bqt4 hul5Δ:: kan^r*	This study	S2, S3A, B
TL267	*h⁻ bqt4Δ::hph bqt3Δ::NAT lys1⁺::bqt4p-GFP-bqt4 dsc1Δ:: kan^r*	This study	S2
TL292	*h⁻ bqt4Δ::hph bqt3Δ::NAT lys1⁺::bqt4p-GFP-bqt4 cut9-665*	This study	S2
TL294	*h⁻ bqt4Δ::hph bqt3Δ::NAT lys1⁺::bqt4p-GFP-bqt4 ptr1-1*	This study	S2

TL235	*h⁻ bqt4Δ::hph bqt3Δ::NAT lys1⁺::bqt4p-GFP-bqt4 doa10Δ::bsd hul5Δ:: kan^r*	This study	S3A, B
TL262	*h⁻ lys1-131 bqt4Δ::hph lys1+::GFP-bqt4C$^{369-425}$ doa10Δ::bsd*	This study	S7

S. cerevisiae strains

Strain	Genotype	Source	Figure
AH109	*MATa*, *trp1-901*, *leu2-3*, *112*, *ura3-52*, *his3-200*, *gal4Δ*, *gal80Δ*, *LYS2*::*GAL1$_{UAS}$-GAL1$_{TATA}$-HIS3*, *MEL1*, *GAL2$_{UAS}$-GAL2$_{TATA}$-ADE2*, *URA3*::*MEL1$_{UAS}$-MEL1$_{TATA}$-lacZ*)	Clontech, Takara Bio	6B
H1N2190	AH109 harboring pGADT7 and pGBKT7	This study	6B
H1N2193	AH109 harboring pGADT7 and pGBKT7-bqt3	This study	6B
H1N2786	AH109 harboring pGADT7-GFP-bqt4(1-432) and pGBKT7	This study	6B
H1N2787	AH109 harboring pGADT7-GFP-bqt4(1-432) and pGBKT7-bqt3	This study	6B
H1N2788	AH109 harboring pGADT7-GFP-bqt4(369-432) and pGBKT7-bqt3	This study	6B
H1N2789	AH109 harboring pGADT7-GFP-bqt4(394-432) and pGBKT7-bqt3	This study	6B
H1N2790	AH109 harboring pGADT7-GFP-bqt4(414-432) and pGBKT7-bqt3	This study	6B
H1N2791	AH109 harboring pGADT7-GFP-bqt4(1-413) and pGBKT7-bqt3	This study	6B
H1N2792	AH109 harboring pGADT7-GFP-bqt4(1-425) and pGBKT7-bqt3	This study	6B
H1N2793	AH109 harboring pGADT7-GFP-bqt4(369-425) and pGBKT7-bqt3	This study	6B
H1N2794	AH109 harboring pGADT7-GFP-bqt4(414-425) and pGBKT7-bqt3	This study	6B
H1N2795	AH109 harboring pGADT7-GFP-bqt4(426-432) and pGBKT7-bqt3	This study	6B

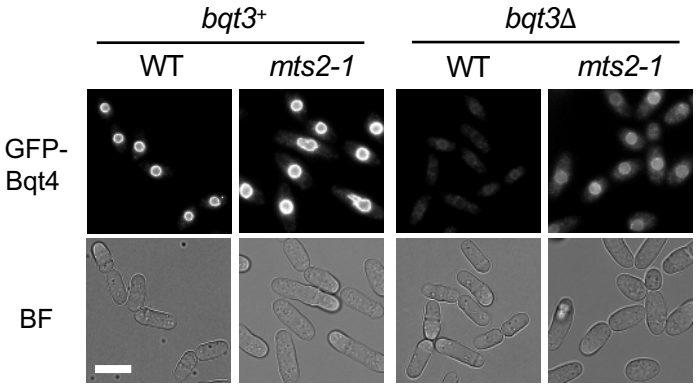

Supplementary Fig. 1. The *mts2-1* mutation prevents Bqt4 degradation
Cells harboring *mts2-1* in the *bqt3*$^{+}$ or *bqt3*Δ background were cultured at a nonpermissive temperature (36°C) for 4 h and observed by fluorescence microscopy. (Upper panels) Fluorescence images of GFP-Bqt4 (lower panels) and bright-field images (BF). Bar: 10 μm.

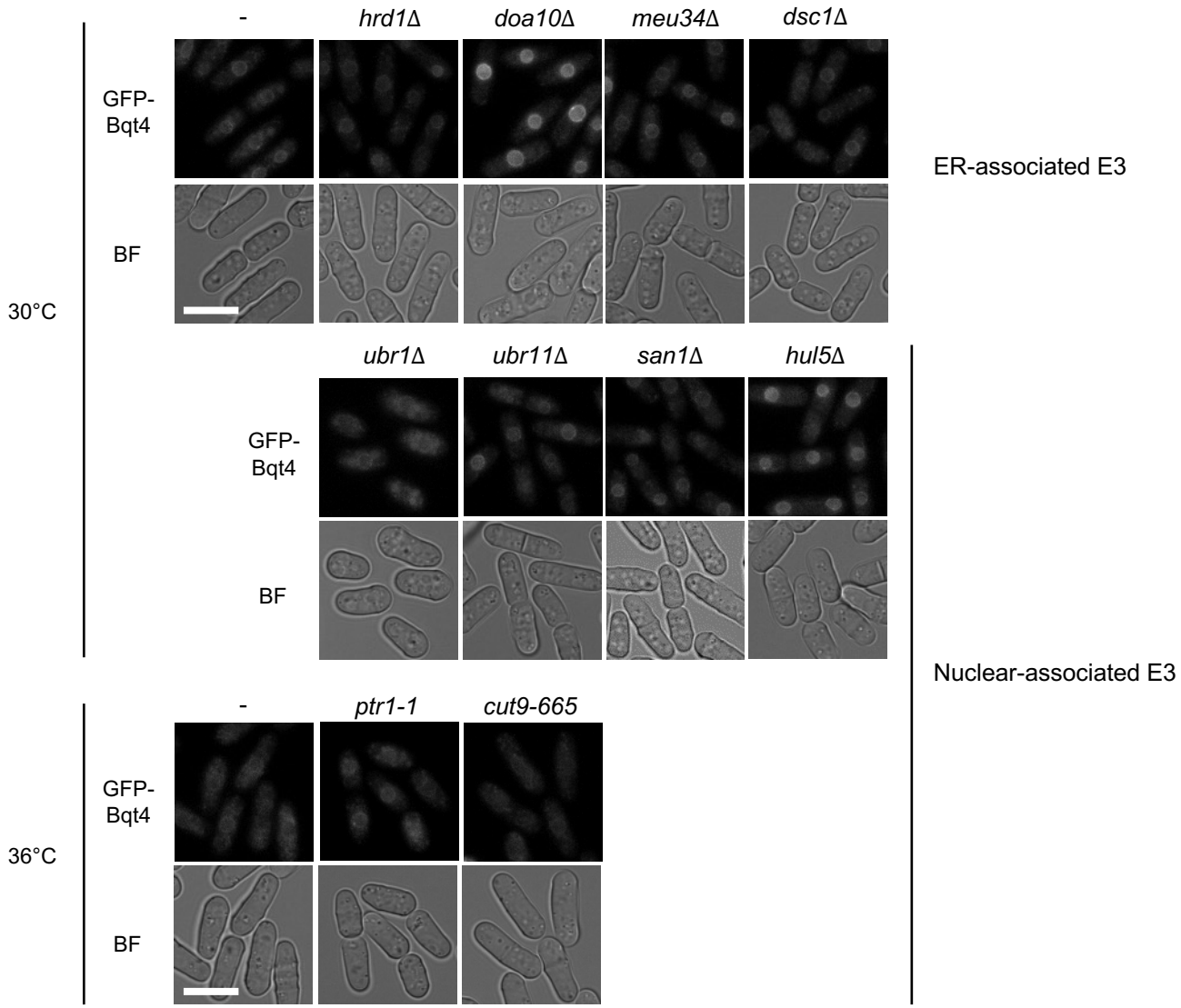

Supplementary Fig. 2. Most nuclear- or ER-associated E3 ligases have a minimal role in Bqt4 degradation

Fluorescence images of GFP-Bqt4 in the mutants are shown. Deletion or mutation of E3 ligases localized in the ER (*meu34*Δ, *dsc1*Δ) or functioning in the nucleus (*san1*Δ, *ubr1*Δ, *ubr11*Δ, *hul5*Δ, *ptr1-1*, *cut9-665*) was introduced in *bqt3*Δ cells expressing GFP-Bqt4. The cells were cultured at 30°C for 16 h or shifted to 36°C for 4 h for *ts* mutants and then observed using fluorescence microscopy. Bars: 10 μm.

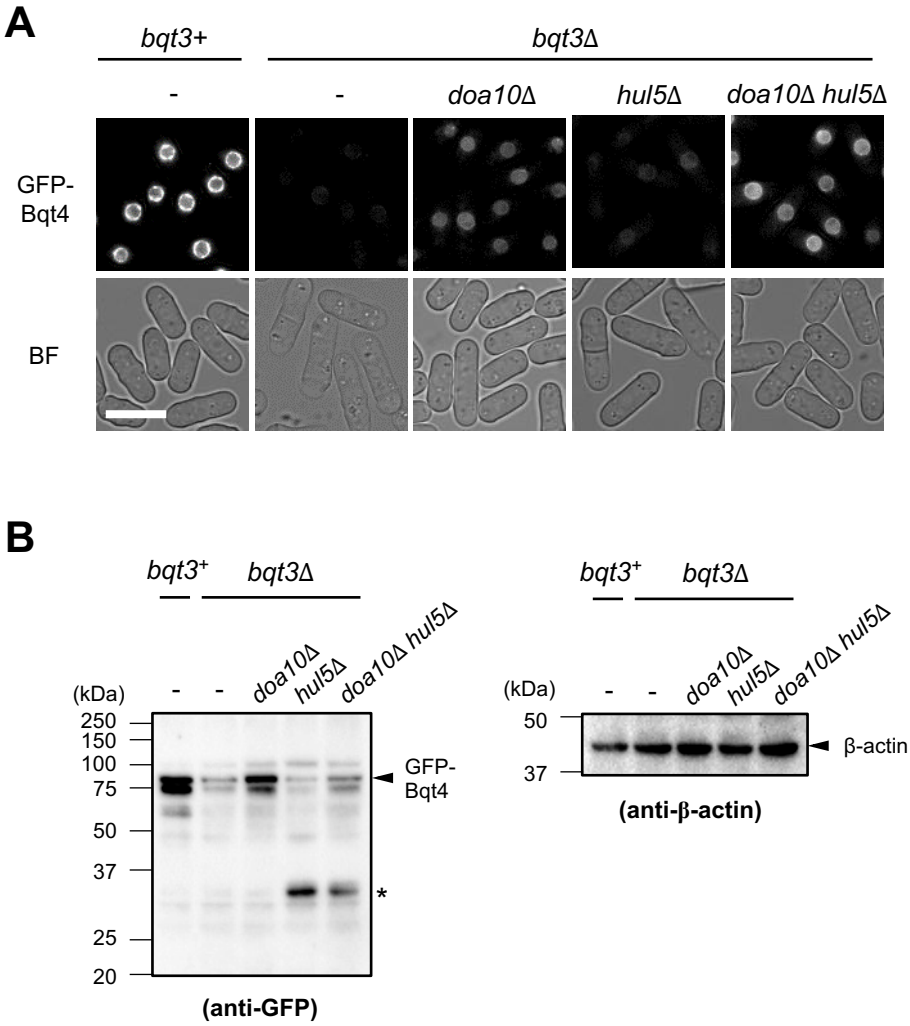

Supplementary Fig. 3. Synthetic effect of double deletion of *doa10* and *hul5* for GFP-Bqt4 level.

Cells harboring the single (*doa10*Δ, *hul5*Δ) or double (*doa10*Δ*hul5*Δ) deletion of ubiquitin E3 ligase in *bqt3*Δ background were cultured at 30° C and subjected to microscopic observation (A) or western blotting (B). (A) Fluorescent images of GFP-Bqt4 mutants are shown. "*bqt3*$^{+}$" shows GFP-Bqt4 level in *bqt3*$^{+}$ cells. BF represents the bright-field image. Bar: 10 μm. (B) Protein levels of GFP-Bqt4 and β-actin were detected by anti-GFP and anti-β-actin antibodies, respectively. The molecular weight markers are shown on the left. The asterisk indicates the degraded product.

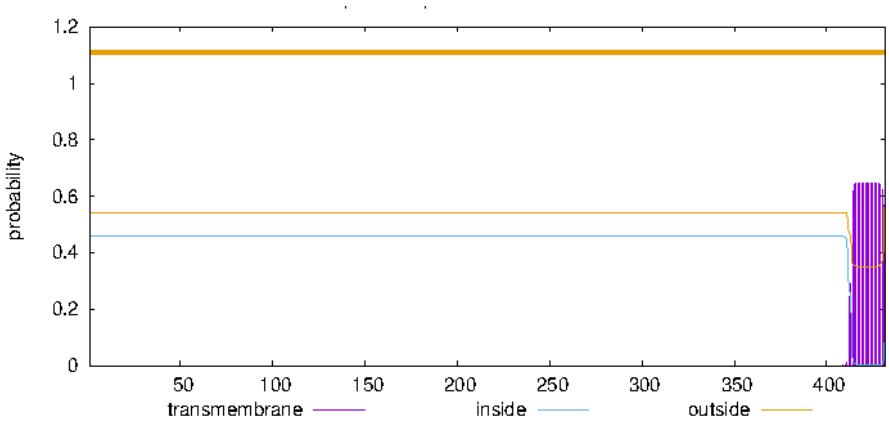

Supplementary Fig. 4. Prediction of Bqt4 TMD properties
The transmembrane helices of Bqt4 were predicted using the TMHMM-2.0 prediction server (https://services.healthtech.dtu.dk/service.php?TMHMM-2.0). The horizontal and vertical axes indicate the prediction probability and amino acid residues of Bqt4, respectively.

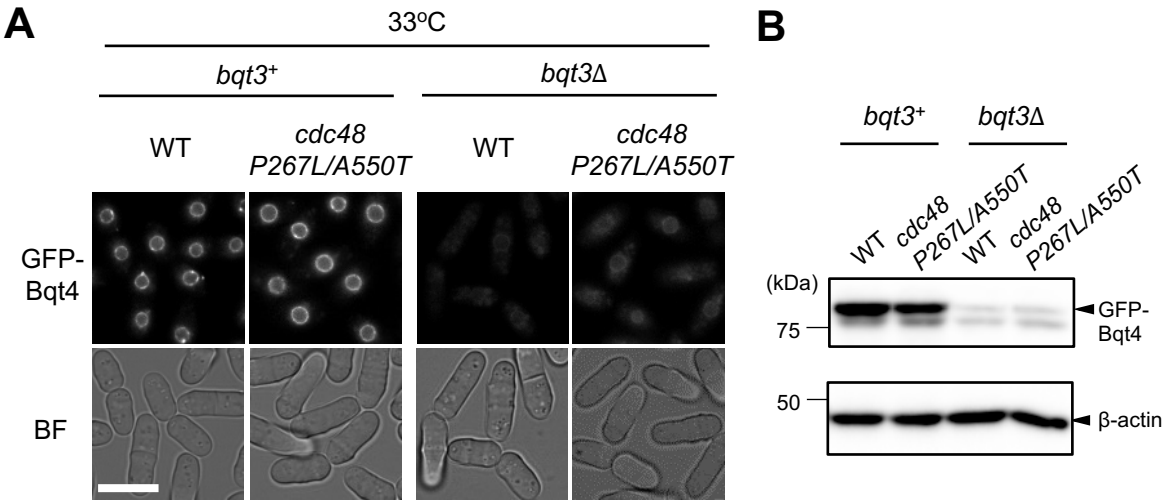

Supplementary Fig. 5. Degradation of Bqt4 is not significantly affected in Cdc48 mutant at the permissive temperature

Cells harboring the cdc48-P267L/A550T mutant in the *bqt3+* or *bqt3Δ* background were cultured at 33° C for 15 h and subjected to microscopic observation (A) or western blotting (B). (A) Fluorescence images of GFP-Bqt4 (upper panels) and bright-field images (lower panels). Bar: 10 μm. (B) The protein levels of GFP-Bqt4 and β-actin were detected by anti-GFP and anti-β-actin antibodies, respectively. The molecular weight markers are shown on the left.

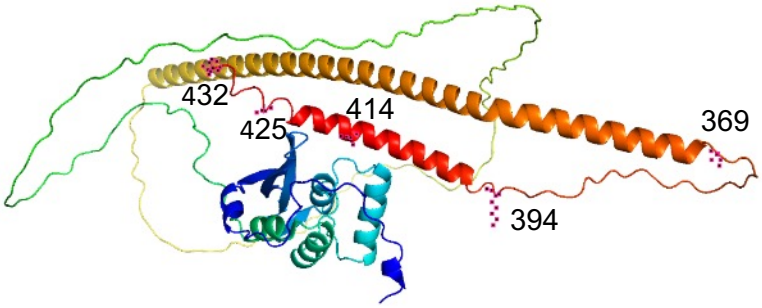

Supplementary Fig. 6. Structure of Bqt4 as predicted by AlphaFold2
The three-dimensional structure of Bqt4 predicted using AlphaFold2 was obtained from the website (https://alphafold.ebi.ac.uk/entry/O60158).

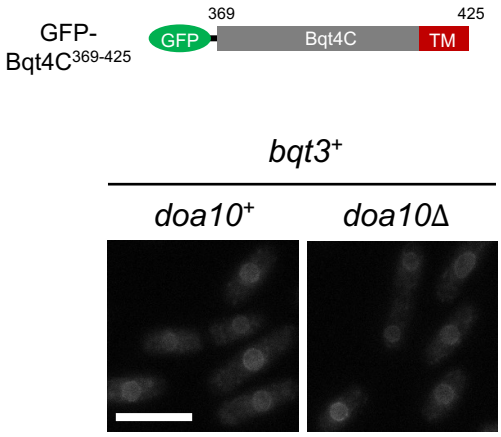

Supplementary Fig. 7. Degradation of Bqt4C$^{369-425}$ occurred independently of Doa10 pathway

The GFP-Bqt4C$^{369-425}$ fragment was expressed in *doa10*$^{+}$ and *doa10*Δ cells and observed by fluorescence microscopy. Scale bar: 10 μm.